

QUIVER NEURAL NETWORKS

JORDAN GANEV ROBIN WALTERS

ABSTRACT. We develop a uniform theoretical approach towards the analysis of various neural network connectivity architectures by introducing the notion of a *quiver neural network*. Inspired by quiver representation theory in mathematics, this approach gives a compact way to capture elaborate data flows in complex network architectures. As an application, we use parameter space symmetries to prove a lossless model compression algorithm for quiver neural networks with certain non-pointwise activations known as *rescaling activations*. In the case of *radial* rescaling activations, we prove that training the compressed model with gradient descent is equivalent to training the original model with projected gradient descent.

1. INTRODUCTION

In recent years, the study of deep neural networks has advanced from the basic case of sequential multilayer perceptrons to incorporating more elaborate structures, including skip connections, multiple inputs with different features pathways, multiple output heads, aggregations, concatenations, and splitting of features. As a result, terms such as ‘layer’ and ‘depth’ come across as insufficiently descriptive for capturing the interdependencies of the hidden feature spaces. In this paper, we propose *quiver neural networks* as a convenient formal tool for schematically describing the data flow in complex network structures.

Our approach stems from representation theory, a branch of mathematics concerned with the formal study of equivariance and symmetry. Representation-theoretic perspectives are increasingly influential in deep learning theory, and have been especially successful in the context of equivariant neural networks, where one exploits symmetries of the input or output spaces, and considers distributions and functions that respect these symmetries [CW16,KT18,RSP17,CW17]. Our techniques, by contrast, focus on parameter space symmetries, and consequently pertain to some degree to all neural networks. Our methods adopt constructions from quiver representation theory, an active research area in mathematics with connections to Lie theory and symplectic geometry [N⁺98,KJ16]. We also build on earlier work applying quiver representation theory to deep learning [ABHR21,AJ20,AJP⁺21,JL21].

Formally, a *quiver* is another term for a finite directed graph. In our constructions, the vertices of the quiver indicate the layers of a neural network architecture, while the edges indicate the data flows interconnecting the layers. A *representation* of a quiver is the assignment of a vector space (i.e., a hidden feature space) to each vertex and a compatible linear map (i.e., a weight matrix) to each edge. Quiver representations, together with a non-linearity at each hidden vertex, combine to produce the structure of a neural network, which we refer to a quiver neural network. Figure 1 illustrates the procedure in the case of a sequential network with three layers.

(IG) Radboud University, Nijmegen, Netherlands. iganev@cs.ru.nl

(RW) Northeastern University, Boston, MA, USA. r.walters@northeastern.edu



FIGURE 1. (Left) An example of a quiver. Each vertex in the top row represents a layer; the bottom vertex is the ‘bias’ vertex. (Right) A quiver neural network. We assign a dimension to each non-bias vertex, linear map to each edge, and an activation to each non-source vertex. When each ρ_i is a pointwise activation, we obtain a three-layer multilayer perceptron.

The formalism of quiver neural networks has several distinct advantages. First, it captures the underlying network connectivity in the simplest possible way, precipitating a uniform analysis of many different data flow architectures including multilayer perceptrons (MLPs) and other basic sequential networks; skip connections; multiple input, output, and internal pathways; aggregations; and others [MYF⁺18, SLD17, HLVDMW17, ZSKS17]. Second, the quiver perspective makes parameter space symmetries more apparent. Specifically, the space of quiver representations has a natural group action; in our formalism, this means one can package the trainable network parameters into a vector space with rich symmetries. Finally, factoring out parameter space symmetries leads to a geometric rephrasing of neural network optimization problems in terms of quiver varieties, where favorable convexity properties are conjectured to exist.

As our main application, we generalize the model compression results of [GvLW22] to quiver neural networks. These results apply to neural networks with *rescaling activations*, rather than usual pointwise activations. Such activations rescale each activation input by a scalar-valued function to produce the activation output. A special class of rescaling activations are *radial* rescaling activations, where the rescaling factor depends only on the norm of the input vector. Neural networks with the radial rescaling version of ReLU (known as Step-ReLU, see Section 4) are universal approximators [GvLW22].

Our model compression algorithm for quiver neural networks with rescaling activations proceeds via iterated QR decompositions over a topological ordering of the vertices. At each layer, one extracts the weights of the compressed model from the upper-triangular matrix ‘ R ’, and uses the orthogonal matrix ‘ Q ’ to modify the activation to a different rescaling function. The output of the algorithm is a quiver neural network with the same underlying quiver, a lower-dimensional feature space at each layer, and new rescaling activations. A key feature of our model compression algorithm is that it is *lossless*: the compressed network has the same value of the loss function on any batch of training data as the original network.

Moreover, we obtain stronger results in the case of radial rescaling activations, which commute orthogonal transformations and hence enjoy special equivariance properties. When the original model has radial activation functions, the compressed model has the same activations restricted to the appropriate subspace; that is, the compression algorithm does not require updating radial rescaling activations. Furthermore, use of radial activations leads to a precise interaction between model compression and training. While training the compressed model via gradient descent does not yield the same result as training the original model, we prove an explicit mathematical relationship between the two procedures, provided that (1) the model has radial rescaling activations

and (2) one trains the original model with *projected gradient descent*. As explained below, projected gradient descent involves zeroing out specific matrix entries after each step of gradient descent. When the compression is significant enough, the compressed model reaches a local minimum faster than the original model.

To summarize, our specific contributions include:

- (1) A theoretical framework for neural networks based on quiver representation theory;
- (2) An implementation of a lossless model compression algorithm for quiver neural networks with rescaling activations.
- (3) A refinement of this algorithm for radial rescaling activations, based on equivariance properties.
- (4) A theorem relating gradient descent optimization of the original and compressed networks, in the case of radial rescaling activations.

Terminology. To avoid ambiguity, we remark on terminology used in this paper. The terms ‘quiver’ and ‘finite directed graph’ are synonymous, but the terms ‘quiver neural network’ and ‘graph neural network’ are distinct. In the latter, the feature spaces are function spaces on the vertex set of a graph [KW16]. By contrast, for quiver neural networks, the feature spaces are not assumed to have any special structure, while the network connectivity (number of layers, interconnections between the layers) is specified by a quiver. Additionally, we do not use the expression ‘representation of a quiver’ in technical sections of the main text, only as background and in the appendix. Instead, we consider the parameter space associated to a quiver.

2. RELATED WORK

Quiver representation theory and neural networks. This work generalizes results in [GvLW22] from the case of basic sequential networks to any quiver neural network (an earlier version of loc. cit. discussed quivers). There has been a number of ground-breaking works relating neural networks to quiver representations [AJ20, ABHR21, AJP⁺21]. As far as we can tell, our current paper strengthens these relations as it (1) captures all architectures appearing thus far, (2) accommodates both pointwise and non-pointwise activation functions, and (3) proves generalizations to larger symmetry groups. Our work is also influenced by algebro-geometric and categorical perspectives placing quiver varieties in the context of neural networks [JL21, MM20]. At the same time, we place more emphasis practical consequences for optimization techniques at the core of machine learning. Our approach also shares parallels with works where quivers are not explicitly mentioned. For example, [WST96] consider neural networks in which each layer is a representation of a finite group, and activations are pointwise; our framework, however, accommodates Lie groups as well as non-pointwise activations. Also, special cases of the “algebraic neural networks” of [PMR] are equivalent to representations of quivers over rings of polynomials. Finally, the study of the “non-negative homogeneity” (or “positive scaling invariance”) property of ReLU activations [DPBB17, NSS15, MZZ⁺19] is a special case of the results appearing in our work.

Rescaling activations. The special case of radial rescaling activations have been studied from several perspectives. Radial rescaling functions have the symmetry property of preserving vector directions, and hence exhibit rotation equivariance. Consequently, examples of such functions, such as the squashing nonlinearity and Norm-ReLU, feature in the study of rotationally equivariant neural networks [WC19, SFH17, WGW⁺18, WHS18, JL21]. From a different direction, in

the vector neurons formalism [DLD⁺21] the output of a nonlinearity is a vector rather than a scalar; rescaling activations are an example. For radial basis networks, each hidden neuron is a radial nonlinear function of the shifted input vector, but the outputs are independent, whereas for rescaling functions, the outputs are also linked together [BL88].

Equivariant neural networks. Representation-theoretic techniques appear in the development of equivariant neural networks; such networks are designed to incorporate symmetry as an inductive bias. In particular, equivariant networks feature weight-sharing constraints based on equivariance or invariance with respect to various symmetry groups. Examples of equivariant architectures include G -convolution, steerable CNN, and Clebsch-Gordon networks [CWKW19, WC19, CW16, CDM18, KT18, BS19, WGTB17, CW17, WHS18, DFK16, LW21, RSP17]. By contrast, the quiver representation theory approach taken in this paper does not depend on symmetries occurring in the input domain, output space, or feedforward mapping. Instead, we exploit parameter space symmetries and thus obtain more general results that apply to domains with no apparent symmetry. From the point of view of model compression, equivariant networks do achieve reduction in the number of trainable parameters through weight-sharing for fixed hidden dimension widths; however, in practice, they may use larger layer widths and consequently have larger memory requirements than non-equivariant models. Sampling or summing over large symmetry groups may make equivariant models computationally slow as well [FSIW20, KT18].

Model compression. Apart from [GvLW22] mentioned above, our method differs significantly from most existing model compression methods [CWZZ17] in that it is based on the inherent symmetry of neural network parameter spaces. One prior model compression method is *weight pruning*, which removes redundant, small, or unnecessary weights from a network with little loss in accuracy [HMD15, BOFG20, Kar90]. Pruning can be done during training or at initialization [FC18, LAGT19, WZG20]. *Gradient-based pruning* identifies low saliency weights by estimating the increase in loss resulting from their removal [LDS90, HS93, DCP17, MTK⁺16]. A complementary approach is *quantization*, in which aims to decrease the bit depth of weights [WLW⁺16, HZC⁺17, GLYB14]. *Knowledge distillation* works by training a small model to mimic the performance of a larger model or ensemble of models [BCNM06, HVD15, BC13]. *Matrix Factorization* methods replace fully connected layers with lower rank or sparse factored tensors [CFF⁺15, CYF⁺15, TXZ⁺15, LGR⁺14, RSLF13, LKZ⁺17] and can often be applied before training. Our method involves a generalized QR decomposition, which is a type of matrix factorization; however, rather than aim for a rank reduction of linear layers, we leverage this decomposition in order to reduce hidden layer widths. Our method shares similarities with lossless compression methods which aim to remove stable or redundant neurons [SYKR21, SKR20], sometimes using symmetry [SZK20]. Finally, while there are similarities between our model compression results and those of [JL21], our results apply to a larger class of activations (beyond the squashing nonlinearity) and feature a group action on all layers (not just disjoint layers).

3. QUIVER NEURAL NETWORKS

3.1. Motivation. What is a neural network? From an abstract point of view, it consists of (1) a connectivity architecture indicating the arrangement and interdependencies of the layers, as well as the data flow, (2) trainable parameters capturing the linear component of the feedforward function, and (3) non-linearities that enhance the expressivity of the feedforward function. As we observe below, the connectivity architecture of a neural network corresponds to a quiver, that

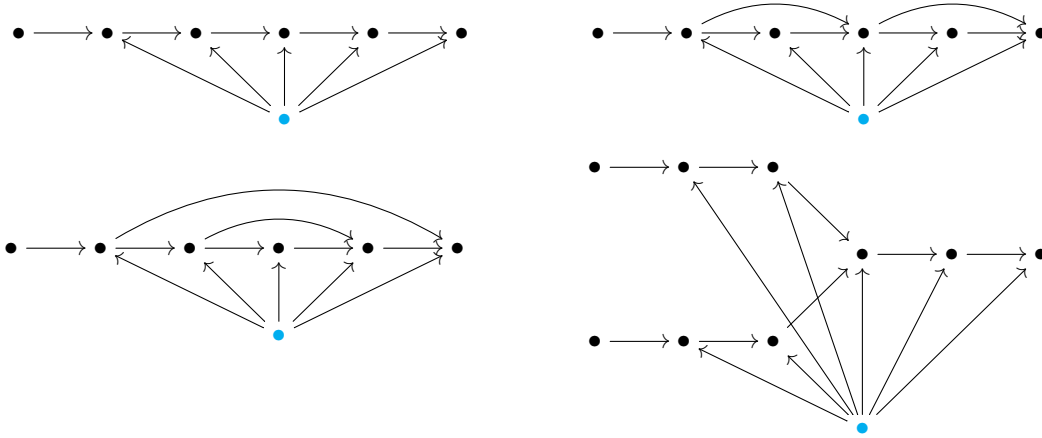


FIGURE 2. Examples of neural quivers. The bias is indicated in blue. Clockwise from top left: the MLP quiver, a quiver with skip connections, a U-net quiver, a quiver defining a network with a "Y" structure.

is, a finite directed graph. Meanwhile, the trainable parameters define a representation of the quiver, that is, a vector space for every vertex and a compatible matrix for every edge. Finally, the non-linearities appear as transformations of the vector space at each vertex. As we will see, this perspective has the advantages of compactly defining the underlying neural network structure, packaging the trainable parameters of a neural network into a vector space, and emphasizing the parameter space symmetries, which are crucial for our results.

3.2. **Quivers.** A *quiver* \mathcal{Q} is a finite directed graph. Thus, a quiver consists of a pair $\mathcal{Q} = (I, E)$, where I is the set of vertices and E is the set of directed edges, together with maps $s : E \rightarrow I$ and $t : E \rightarrow I$ indicating the source and target of each edge. As usual, a *source* in \mathcal{Q} is a vertex with no incoming edges, and a *sink* is a vertex with no outgoing edges. A *dimension vector* for a quiver is the assignment of a dimension d_i to each vertex i ; we group these into a tuple $\mathbf{d} = (d_i)_{i \in I}$ of positive integers indexed by the vertices.

3.3. **Neural quivers.** We define the general class of quivers relevant to neural networks and machine learning. A *neural quiver* is a connected acyclic quiver $\mathcal{Q} = (I, E)$, together with a distinguished vertex $i_{\text{bias}} \in I$, called the *bias vertex*, satisfying the following condition: The bias vertex i_{bias} is a source, and removing i_{bias} creates no new sources in \mathcal{Q} . The condition on the bias vertex guarantees that every non-source vertex admits a path from a non-bias source vertex. We note that all results have versions in the simpler case of no bias, and any connected acyclic quiver with more than one vertex can be extended to the structure of a neural quiver by adding an extra source vertex to play the role of the bias. A vertex of a neural quiver is called *hidden* if it is neither a source nor a sink. Let I_{hidden} denote the set of hidden vertices. Since any neural quiver is acyclic, it admits a *topological order* of its vertices, i.e., an enumeration $I = \{i_1, \dots, i_{|I|}\}$ of the vertex set such that, if there is an edge from i_n to i_m , then $n < m$. In many of the constructions that appear below, one must fix a topological order; however, the particular choice of topological order is irrelevant.

3.4. Quiver neural networks. We now state the definition of a quiver neural network. Let $\mathcal{Q} = (I, E)$ be a neural quiver. A \mathcal{Q} -neural network consists of a dimension d_i for each vertex $i \in I$, with $d_{i_{\text{bias}}} = 1$; a weight matrix $W_e \in \mathbb{R}^{d_{t(e)} \times d_{s(e)}}$ for every edge $e \in E$; and an activation $\rho_i : \mathbb{R}^{d_i} \rightarrow \mathbb{R}^{d_i}$ for every non-source vertex i . We group the dimensions, weight matrices, and activations into tuples: $\mathbf{d} = (d_i)_{i \in I}$, $\mathbf{W} = (W_e)_{e \in E}$, and $\boldsymbol{\rho} = (\rho_i)_{i \in I}$ where, for convenience, we set ρ_i to be the identity if i is a source vertex. Hence, we denote a \mathcal{Q} -neural network as a triple of tuples: $(\mathbf{d}, \mathbf{W}, \boldsymbol{\rho})$. The tuple \mathbf{d} is a dimension vector for \mathcal{Q} . Note that the ‘weight matrix’ assigned to an edge from the bias vertex to a vertex i is of size $d_i \times 1$, so it is a column vector, or, equivalently, an element of \mathbb{R}^{d_i} . Examples of quiver neural networks include:

- (1) Sequential quivers, see Figure 1 and Figure 2, top left. In Figure 1, the weight matrix W_i is of size $d_i \times d_{i-1}$, and the ‘matrix’ b_i corresponds to an element of \mathbb{R}^{d_i} . Each activation ρ_i is a non-linear map from \mathbb{R}^{d_i} to itself. When the activation functions are pointwise, the resulting quiver neural network is nothing more than an MLP.
- (2) ResNet quivers, see Figure 2, top right and bottom left. These quivers have skip-connections, and the resulting quiver neural networks are examples of ResNets.
- (3) Multiple inputs are possible, as in Figure 2, bottom right. For example, Y-nets are captured by our formalism [MYF⁺18].
- (4) U-nets have been studied in [SLD17], and are also examples of quiver neural networks, as indicated in Figure 2 bottom left¹.

3.5. The feedforward function. To define the feedforward function of a quiver neural network $(\mathbf{d}, \mathbf{W}, \boldsymbol{\rho})$, we require some additional terminology. We call any source vertex that is not the bias an *input* vertex, and any sink vertex an *output* vertex. Thus, the vertex set I is the disjoint union of $\{i_{\text{bias}}\}$, $\{\text{input vertices}\}$, $\{\text{output vertices}\}$, and I_{hidden} .

Given a dimension vector \mathbf{d} for \mathcal{Q} , set: $d_{\text{in}} = \sum_{i \in \{\text{inputs}\}} d_i$ and $d_{\text{out}} = \sum_{i \in \{\text{outputs}\}} d_i$. Hence, we identify $\mathbb{R}^{d_{\text{in}}}$ with the direct sum of the spaces \mathbb{R}^{d_i} as i ranges over the input vertices, and similarly for $\mathbb{R}^{d_{\text{out}}}$. Next, fix a topological order of the vertices. For every vertex $i \in I$, define a function: $F_i : \mathbb{R}^{d_{\text{in}}} \rightarrow \mathbb{R}^{d_i}$ recursively as follows. If i is a source, then F_i is the projection map. If $i = i_{\text{bias}}$ is the bias vertex, then $F_i \equiv 1$ is the constant function at $1 \in \mathbb{R} = \mathbb{R}^{d_{i_{\text{bias}}}}$. For all other vertices, we use the recursive definition:

$$F_i(x) = \rho_i \left(\sum_{j \xrightarrow{e} i} W_e \circ F_j(x) \right).$$

That is, to compute the hidden feature at node i , first loop over the incoming edges to i , applying the weight matrix for each edge to the feature vector at the source vertex of the edge; next, sum the results (which are all elements of \mathbb{R}^{d_i}); and, finally, apply the activation. The definitions of the F_i are independent of the choice of topological order, as is the following definition: The *feedforward function* $F = F_{(\mathbf{d}, \mathbf{W}, \boldsymbol{\rho})} : \mathbb{R}^{d_{\text{in}}} \rightarrow \mathbb{R}^{d_{\text{out}}}$ of the neural network $(\mathbf{d}, \mathbf{W}, \boldsymbol{\rho})$ is defined as $F(x) = (F_i(x))_{i \in \{\text{output vertices}\}}$.

¹At least the non-convolutional versions thereof. We expect the quiver formalism to generalize to convolutional neural networks.

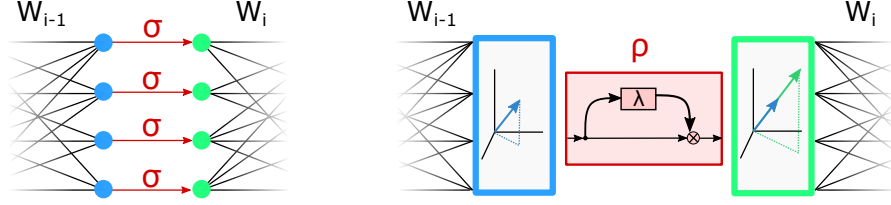


FIGURE 3. Figure 1: (Left) Pointwise activations distinguish a specific basis of each hidden layer and treat each coordinate independently. (Right) Rescaling activations rescale each feature vector by a scalar-valued function λ .

4. RESCALING ACTIVATIONS AND QR MODEL COMPRESSION

In this section, we state a model compression result for quiver neural networks in which each activation belongs to a certain class of non-pointwise activations, known as a rescaling activations. We also consider the case of radial rescaling activations, which commute with orthogonal transformations. Proofs appear in Appendix A.

4.1. Rescaling activations. A function $\rho : \mathbb{R}^d \rightarrow \mathbb{R}^d$ is said to be *rescaling* if it sends each vector to a scalar multiple itself, that is:

$$\rho(v) = \lambda(v)v \quad \text{for all } v \in \mathbb{R}^d$$

for some scalar-valued function $\lambda : \mathbb{R}^d \rightarrow \mathbb{R}$. We say that a \mathcal{Q} -neural network $(\mathbf{d}, \mathbf{W}, \rho)$ has *rescaling activations* if each $\rho_i : \mathbb{R}^{d_i} \rightarrow \mathbb{R}^{d_i}$ is a rescaling function. Examples include: (1) Step-ReLU, where the rescaling factor $\lambda(v)$ is equal to 0 if the vector v is of norm less than one, and 1 if v of norm at least one. Fully-connected MLPs with Step-ReLU activations are known to be universal approximators [GvLW22]. (2) $\lambda(v) = |v - c|$ for some $c \in \mathbb{R}^d$.

4.2. Reduced dimension vector. Let \mathbf{d} be a dimension vector for an acyclic quiver \mathcal{Q} . The *reduced dimension vector* \mathbf{d}^{red} associated to \mathbf{d} is defined as follows, using a topological order of the vertices. If i is a source or sink vertex, then $d_i^{\text{red}} = d_i$. Otherwise, d_i^{red} is the minimum of d_i and the sum $d_{\rightarrow i}^{\text{red}} = \sum_{j \rightarrow i} d_j^{\text{red}}$ of the values of the reduced dimension vector at all the vertices with an outgoing edge to i :

$$d_i^{\text{red}} = \min(d_i, d_{\rightarrow i}^{\text{red}}).$$

This definition is independent of the choice of topological order. Since $d_i^{\text{red}} \leq d_i$, let $\text{Inc}_i : \mathbb{R}^{d_i^{\text{red}}} \hookrightarrow \mathbb{R}^{d_i}$ be the inclusion into the first d_i^{red} coordinates; as a matrix, it has ones along the diagonal and zeros elsewhere. Let $\pi_i : \mathbb{R}^{d_i} \rightarrow \mathbb{R}^{d_i^{\text{red}}}$ be the projection onto the first d_i^{red} coordinates.

4.3. Model compression. In this section, we give a model compression result for quiver neural networks with radial activations. The result is based on Algorithm 1, whose input is a quiver neural network rescaling activations and whose output is a quiver neural network with smaller widths (and the same underlying quiver). Specifically, if the original widths are given by the dimension vector \mathbf{d} , then the compressed widths are given by the reduced dimension vector \mathbf{d}^{red} . The algorithm proceeds by computing successive QR decompositions according to a topological order of the vertices. The resulting upper-triangular matrix leads to the reduced weights, while

Algorithm 1: QR Model Compression for Rescaling activations (QR-Compress)

```

input   :  $\mathcal{Q}$ -neural network  $(\mathbf{d}, \mathbf{W}, \rho)$  with each  $\rho_i$  rescaling
output  :  $\mathcal{Q}$ -neural network  $(\mathbf{d}^{\text{red}}, \mathbf{W}^{\text{red}}, \tau)$ , orthogonal matrices  $\mathbf{Q} = (Q_i \in O(d_i))_{i \in I_{\text{hidden}}}$ 
 $\mathbf{Q}, \mathbf{W}^{\text{red}}, \tau \leftarrow [], [], []$  // initialize output matrix lists
 $I = \text{top\_sort}(I)$  // topological order of vertices
for  $i$  in  $I$  do
     $M_i \leftarrow \text{hstack}(W_e Q_{s(e)} \text{Inc}_{s(e)} : t(e) = i)$  // merge transf. incoming weights
    if  $i$  is not a source or a sink then
         $Q_i, R_i \leftarrow \text{QR-decomp}(M_i, \text{mode} = \text{'complete'})$  //  $M_i = Q_i \text{Inc}_i R_i$ 
         $\tau_i \leftarrow \pi_i \circ Q_i^{-1} \circ \rho_i \circ Q_i \circ \text{Inc}_i$  // update activations
        Append  $Q_i$  to  $\mathbf{Q}$ 
        Append  $\tau_i$  to  $\tau$ 
    else if  $i$  is sink then
         $R_i \leftarrow M_i$ 
        Append  $\rho_i$  to  $\tau$  // unchanged output activations
    for  $e$  such that  $t(e) = i$  do
         $W_e^{\text{red}} \leftarrow \text{extract}(R_i, e)$  // extract columns corresp. to  $e$ 
        Append  $W_e^{\text{red}}$  to  $\mathbf{W}^{\text{red}}$  // reduced weights
    end
end
return  $(\mathbf{d}^{\text{red}}, \mathbf{W}^{\text{red}}, \tau)$ , and  $\mathbf{Q}$ 

```

Notes: The method QR-decomp returns the complete QR decomposition of the $d_i \times d_{\rightarrow i}^{\text{red}}$ matrix M_i as $Q_i \text{Inc}_i R_i$ where $Q_i \in O(d_i)$ is an orthogonal $d_i \times d_i$ matrix and R_i is upper-triangular of size $d_i^{\text{red}} \times d_{\rightarrow i}^{\text{red}}$. The method top_sort produces a topological order, the method hstack concatenates matrices horizontally, and the method extract applied to (R_i, e) extracts from R_i the $d_{s(e)}^{\text{red}}$ columns corresponding to the edge e .

the resulting orthogonal matrix provides a change-of-basis for the feature spaces and is used to update the rescaling activations to new rescaling activations.

Theorem 4.1. *Algorithm 1 is a lossless model compression algorithm. More precisely, the input and output \mathcal{Q} -neural networks of Algorithm 1 have the same feedforward function.*

While a full proof appears in Appendix A, we now give a brief description of the ideas behind the proof. Let i be a hidden vertex. Consider the subspace \mathcal{V}_i of the feature space \mathbb{R}^{d_i} spanned by the images of the linear maps W_e corresponding to the incoming edges. Rescaling activations preserve subspaces, so the subspace \mathcal{V}_i is sent to itself under the activation ρ_i . Hence, if \mathcal{V}_i is a proper subspace (i.e., not all of \mathbb{R}^{d_i}), then one can ignore elements in \mathbb{R}^{d_i} not in \mathcal{V}_i and reduce d_i to the dimension of \mathcal{V}_i . One must subsequently rewrite the matrices W_i in a basis for \mathcal{V}_i ; the QR decomposition provides a convenient way to do this. The resulting orthogonal matrix Q_i is not relevant for the statement of Theorem 4.1, but features in the proof and in Section 5.

We remark on refinements and improvements to Algorithm 1 and Theorem 4.1; see Appendix A for more details. First, if each merged matrix M_i is of full rank, as is practically always the case with random initialization, then no further lossless compression beyond the dimension vector

\mathbf{d}^{red} is possible. In fact, there is a precise sense in which the compressed model is the *minimal subnetwork* of the original model with the same feedforward function (Appendix A.4). However, in situations where M_i are not assumed to be of full rank, Algorithm 1 can be improved to compress to a model with even narrower widths (Appendix A.2). Finally, if one allows for changing the basis of the output space, then one can set d_i^{red} equal to $\min(d_i, d_{\rightarrow i}^{\text{red}})$ for output vertices. This is due to the fact that the common feedforward function of the compressed and original models lies in a subspace of $\mathbb{R}^{d_{\text{out}}}$ of dimension $\sum_{i \in \text{sinks}} \min(d_i, d_{\rightarrow i}^{\text{red}})$.

4.4. Radial neural networks. We now consider a special class of rescaling functions with favorable equivariance properties. A *radial rescaling function* is a rescaling function of the form

$$\rho : \mathbb{R}^d \rightarrow \mathbb{R}^d, \quad v \mapsto \frac{h(|v|)}{|v|}v$$

for a function $h : \mathbb{R} \rightarrow \mathbb{R}$. In other words, the rescaling factor $\lambda(v) = \frac{h(|v|)}{|v|}$ depends only on the norm. Radial rescaling functions commute with orthogonal transformations, and in fact they are precisely the rescaling activations that do so (Lemma A.5). Examples include: (1) Step-ReLU, discussed above. (2) The squashing function, where $h(r) = \frac{r^2}{r^2+1}$. (3) Shifted ReLU, where $h(r) = \text{ReLU}(r - b)$ for $r > 0$ and a real number b . We refer to [GvLW22, WC19] and the references therein for more examples and discussion of radial functions.

Let $\mathcal{Q} = (I, E)$ be a neural quiver. We say that a \mathcal{Q} -neural network $(\mathbf{d}, \mathbf{W}, \rho)$ is a *radial \mathcal{Q} -neural network* if each ρ_i is a radial rescaling activation. The following result is a straightforward consequence of the fact that ρ_i commutes with orthogonal transformations, and implies that one can simplify Algorithm 1 in the case of radial rescaling activations.

Proposition 4.2. *For radial \mathcal{Q} -neural networks, Algorithm 1 leaves the activation functions unchanged.*

5. PROJECTED GRADIENT DESCENT

In practice, one typically applies a compression algorithm to a fully trained model in order to produce a smaller model that is more efficient at deployment. Some compression algorithms also accelerate training; this is the case, for example, when the compressed and original models have the same feedforward function after a step of gradient descent is applied to each. Unfortunately, for quiver neural networks with rescaling activations, compression using Algorithm 1 before training does not yield the same result as training followed by compression (even in the basic sequential case with radial rescaling activations [GvLW22]). There is, however, an explicit mathematical relationship between optimization of the two networks, assuming radial rescaling activations. Namely, as we discuss in this section, the loss of the compressed model after one step of gradient descent coincides with to the loss of a transformation of the original model after one step of *projected* gradient descent. We emphasize that the results of this section only hold for radial rescaling functions (which commute with orthogonal transformations), not general rescaling functions. Proofs of the results of this section appear in Appendix B.

5.1. Parameter space symmetries. To state our results, we introduce additional notation. Let \mathcal{Q} be a quiver and \mathbf{d} a dimension vector for \mathcal{Q} . Set:

$$\text{Param}(\mathcal{Q}, \mathbf{d}) = \bigoplus_{e \in E} \mathbb{R}^{d_{t(e)} \times d_{s(e)}} \quad \text{and} \quad O(\mathbf{d}^{\text{hid}}) = \prod_{i \in I_{\text{hidden}}} O(d_i)$$

to be the corresponding *space of trainable parameters*² and *orthogonal symmetry group*, respectively. Note that each tuple of weight matrices \mathbf{W} in a \mathcal{Q} -neural network belongs to $\text{Param}(\mathcal{Q}, \mathbf{d})$. An element of the orthogonal symmetry group consists of the choice of an orthogonal transformation of \mathbb{R}^{d_i} for each hidden vertex i , and results in a corresponding transformation of the weight matrices W_e appearing in any element \mathbf{W} . To be explicit, a particular choice $\mathbf{Q} = (Q_i)_i$ of orthogonal matrices results in the following linear transformation of weight matrices:

$$\mathbf{W} \mapsto \mathbf{Q} \cdot \mathbf{W} = \left(Q_{t(e)} \circ W_e \circ Q_{s(e)}^{-1} \right)_e$$

Hence we obtain a linear action of $O(\mathbf{d}^{\text{hid}})$ on $\text{Param}(\mathcal{Q}, \mathbf{d})$. It is straightforward to show that, when using radial rescaling activations, this action leaves the feedforward function unchanged (analogous to the ‘positive scaling invariance’ property of ReLU [DPBB17, NSS15, MZZ+19]).

5.2. Gradient descent maps. Fix a neural quiver $\mathcal{Q} = (I, E)$, a dimension vector \mathbf{d} , and a tuple of radial rescaling activations $\rho = (\rho_i : \mathbb{R}^{d_i} \rightarrow \mathbb{R}^{d_i})_{i \in I}$ (where, as usual, ρ_i is the identity if i is a source). For any batch of training data $\{(x_j, y_j)\} \subseteq \mathbb{R}^{d_{\text{in}}} \times \mathbb{R}^{d_{\text{out}}}$, we have the loss function $\mathcal{L} : \text{Param}(\mathcal{Q}, \mathbf{d}) \rightarrow \mathbb{R}$ taking \mathbf{W} to $\sum_j \mathcal{C}(F_{(\mathbf{d}, \mathbf{W}, \rho)}(x_j), y_j)$, where $\mathcal{C} : \mathbb{R}^{d_{\text{out}}} \times \mathbb{R}^{d_{\text{out}}} \rightarrow \mathbb{R}$ is a cost function on the output space. For a learning rate $\eta > 0$, the corresponding gradient descent map on $\text{Param}(\mathcal{Q}, \mathbf{d})$ is given by:

$$\gamma : \text{Param}(\mathcal{Q}, \mathbf{d}) \rightarrow \text{Param}(\mathcal{Q}, \mathbf{d}) \quad \mathbf{W} \mapsto \mathbf{W} - \eta \nabla_{\mathbf{W}} \mathcal{L}.$$

Similarly, using the reduced dimension vector, we have the loss function $\mathcal{L}_{\text{red}} : \text{Param}(\mathcal{Q}, \mathbf{d}^{\text{red}}) \rightarrow \mathbb{R}$ and gradient descent map γ_{red} on $\text{Param}(\mathcal{Q}, \mathbf{d}^{\text{red}})$ given by $\mathcal{L}_{\text{red}}(\mathbf{X}) = \sum_j \mathcal{C}(F_{(\mathbf{d}^{\text{red}}, \mathbf{X}, \rho^{\text{red}})}(x_j), y_j)$ and $\gamma_{\text{red}}(\mathbf{X}) = \mathbf{X} - \eta \nabla_{\mathbf{X}} \mathcal{L}_{\text{red}}$, respectively.

Next we define the projected gradient descent map. Fix a dimension vector \mathbf{d} for the neural quiver \mathcal{Q} . The *projected gradient descent* map on the parameter space $\text{Param}(\mathcal{Q}, \mathbf{d})$ is defined as:

$$\gamma_{\text{proj}} : \text{Param}(\mathcal{Q}, \mathbf{d}) \rightarrow \text{Param}(\mathcal{Q}, \mathbf{d}) \quad \mathbf{W} \mapsto \text{Proj}(\mathbf{W} - \eta \nabla_{\mathbf{W}} \mathcal{L})$$

where $\text{Proj} : \text{Param}(\mathcal{Q}, \mathbf{d}) \rightarrow \text{Param}(\mathcal{Q}, \mathbf{d})$ is the map that zeros out all entries in the bottom left $(d_{t(e)} - d_{t(e)}^{\text{red}}) \times d_{s(e)}^{\text{red}}$ submatrix of each $W_e - \eta \nabla_{W_e} \mathcal{L}$. Schematically:

$$(\mathbf{W} - \eta \nabla_{\mathbf{W}} \mathcal{L})_e = W_e - \eta \nabla_{W_e} \mathcal{L} = \begin{bmatrix} * & * \\ * & * \end{bmatrix} \mapsto \text{Proj}(\mathbf{W} - \eta \nabla_{\mathbf{W}} \mathcal{L})_e = \begin{bmatrix} * & * \\ 0 & * \end{bmatrix}$$

where we regard $\mathbf{W} - \eta \nabla_{\mathbf{W}} \mathcal{L}$ as a tuple $(W_e - \eta \nabla_{W_e} \mathcal{L})_{e \in E} \in \text{Param}(\mathcal{Q}, \mathbf{d})$. Hence, while all entries of each matrix W_e in the tuple \mathbf{W} contribute to the computation of the gradient $\nabla_{\mathbf{W}} \mathcal{L}$, only those not in the bottom left submatrix get updated under the projected gradient descent map γ_{proj} , while those in the bottom left submatrix are zeroed out.

We are now ready to state the relationship between gradient descent on the compressed model and projected gradient descent on the original model. Let \mathbf{W} be a tuple in $\text{Param}(\mathcal{Q}, \mathbf{d})$. Applying Algorithm 1, let $\mathbf{W}^{\text{red}} \in \text{Param}(\mathcal{Q}, \mathbf{d}^{\text{red}})$ be the reduced parameters and $\mathbf{Q} \in O(\mathbf{d}^{\text{hid}})$ the orthogonal symmetries. Set $\mathbf{T} = \mathbf{Q}^{-1} \cdot \mathbf{W}$ to be the transformed parameters, so that $\mathbf{W} = \mathbf{Q} \cdot \mathbf{T}$.

Theorem 5.1. *Let $\mathbf{W} \in \text{Param}(\mathcal{Q}, \mathbf{d})$, and let $\mathbf{W}^{\text{red}}, \mathbf{Q}, \mathbf{T}$ be as above. For any $k \geq 0$, we have³:*

$$\gamma^k(\mathbf{W}) = \mathbf{Q} \cdot \gamma^k(\mathbf{T}) \quad \gamma_{\text{proj}}^k(\mathbf{T}) = \gamma_{\text{red}}^k(\mathbf{W}^{\text{red}}) + (\mathbf{T} - \mathbf{W}^{\text{red}}).$$

²A choice of trainable parameters is the same as a representation of the quiver, see Appendix C.

³More precisely, the second equality is $\gamma_{\text{proj}}^k(\mathbf{T}) = \iota(\gamma_{\text{red}}^k(\mathbf{W}^{\text{red}})) + \mathbf{T} - \iota(\mathbf{W}^{\text{red}})$ where $\iota : \text{Param}(\mathcal{Q}, \mathbf{d}^{\text{red}}) \hookrightarrow \text{Param}(\mathcal{Q}, \mathbf{d})$ is the natural inclusion. See Appendix B.

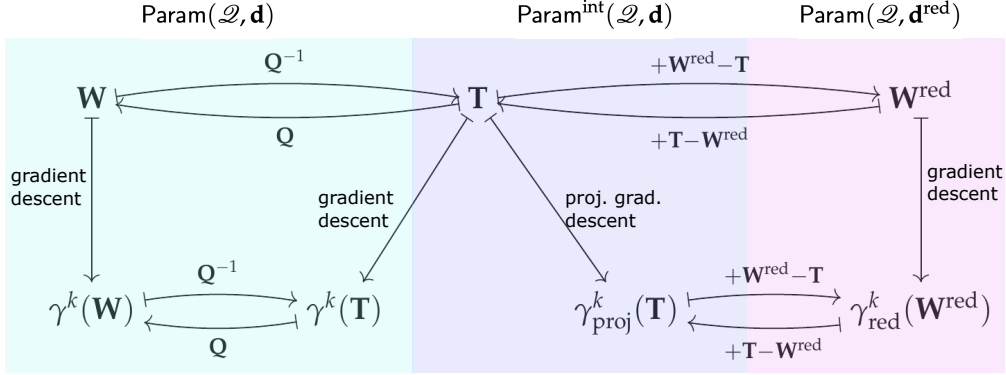


FIGURE 4. Schematic summary of Theorem 5.1. The left horizontal maps indicate the action of $\mathbf{Q}^{\pm 1}$, the right horizontal maps indicate translation by $\pm(\mathbf{T} - \mathbf{W}^{\text{red}})$, and the vertical maps are various versions of gradient descent. The colored regions indicate the (smallest) vector space to which the various tuples naturally belong; the interpolating subspace $\text{Param}^{\text{int}}(\mathcal{Q}, \mathbf{d})$ is defined in Appendix B.

Hence, the gradient descent optimization of the original model \mathbf{W} and the transformed model \mathbf{T} are equivalent, since at any stage they are related by the orthogonal change-of-basis action of \mathbf{Q} . Meanwhile, optimization of the transformed model \mathbf{T} via projected gradient descent is equivalent to the gradient descent optimization of the compressed model \mathbf{W}^{red} , since at any stage one can add or subtract the quantity $\mathbf{T} - \mathbf{W}^{\text{red}}$ to obtain one from the other. Note that, for $k \geq 0$, we have the k -fold composition $\gamma^k = \gamma \circ \gamma \circ \dots \circ \gamma$ and similarly for γ_{red} and γ_{proj} . We summarize Theorem 5.1 in Figure 4 and give a proof in Appendix B.

6. EXPERIMENTS

We provide a software package making it easy to build quiver neural networks by simply specifying the quiver \mathcal{Q} , the dimension vector, and the activation functions. We also implement the model compression algorithm 1. As a check for our theoretical results we provide empirical verification of the above theorems. For simplicity, our experiments only consider the case of radial rescaling activations.

Empirical verification of Theorem 4.1. We consider the quivers displayed in Figure 5. We write dimension vectors as a list according to alphabetic order of the vertices (which is also a topological order), that is, as (d_a, d_b, d_c, \dots) . We select the following dimension vectors: $(2, 4, 8, 2)$, $(1, 2, 8, 2, 6)$, and $(2, 4, 4, 8, 2)$, respectively. The corresponding reduced dimension vectors are: $(2, 3, 6, 2)$, $(1, 2, 4, 2, 6)$, and $(2, 3, 3, 7, 2)$. The weights, biases, inputs, and labels are randomly assigned from $\text{Uniform}([0, 1])$. Over 10 trials, the feedforward functions of the original and compressed models agree up to machine precision: $|F_{\text{orig}} - F_{\text{compressed}}| < 10^{-6}$.

Empirical verification of Theorem 5.1. We verify the theorem for the three quivers appearing in Figure 5. Over 10 trials, one step of gradient descent of the compressed model matches one step of projected gradient descent of the original model up to machine precision:

$$|\gamma(\mathbf{W}) - \mathbf{Q} \cdot \gamma(\mathbf{T})| < 10^{-5} \quad |\gamma_{\text{proj}}(\mathbf{T}) + \mathbf{W}^{\text{red}} - \gamma_{\text{red}}(\mathbf{W}^{\text{red}}) - \mathbf{T}| < 10^{-6}$$

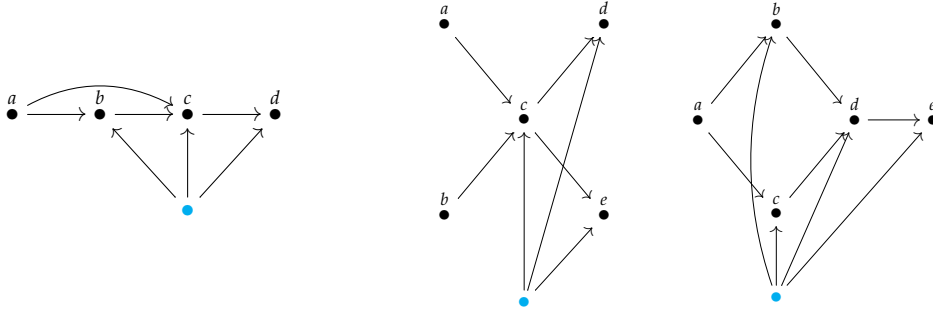


FIGURE 5. Quivers used in the experiments of Section 6. The alphabetical order of the vertices is a topological order. As usual, the bottom vertex is the bias vertex.

7. CONCLUSIONS AND FUTURE WORK

In this paper, we propose a new formalism for the study of neural network connectivity and data flows via the notion of a quiver neural network. While many of our constructions originate in the somewhat abstract mathematical domain of quiver representation theory, we argue that there are practical advantages to quiver neural networks. Namely, our formalism captures connectivity architectures in the simplest possible way, emphasizes parameter space symmetries, leads to an explicit lossless model compression algorithm, and links the compression to gradient descent optimization.

Moreover, our work opens a number of directions for future work. First, a modification of our techniques may lead to a generalization of Algorithm 1 beyond rescaling activations to certain other families of non-pointwise activations. Second, we expect our framework to extend to encapsulate equivariant and convolutional neural networks. Third, our constructions are compatible with various regularization techniques (particularly L_2 -regularization); we have not yet explored the practical consequences of this compatibility. Fourth, future work would include an evaluation of empirical performance on real-world data sets. Finally, a natural next theoretical step would be to explore relations with quiver varieties and reformulate optimization problems geometrically, with the aim to obtain better convexity properties of the appropriate version of the loss function.

ACKNOWLEDGEMENTS

We are grateful for valuable feedback and suggestions from Avraham Aizenbud, Rustam Antia, Marco Antonio Armenta, Niklas Smedemark-Margulies, Jan-Willem van de Meent, Twan van Laarhoven, and Rose Yu. This work was partially funded by the NWO under the CORTEX project (NWA.1160.18.316) and NSF grant #2134178. Robin Walters is supported by the Roux Institute and the Harold Alfond Foundation.

REFERENCES

- [ABHR21] Marco Armenta, Thomas Brüstle, Souheila Hassoun, and Markus Reineke, *Double framed moduli spaces of quiver representations*, arXiv:2109.14589 [cs, math] (October 2021). arXiv: 2109.14589. [↑1, 3](#)
- [AJ20] Marco Antonio Armenta and Pierre-Marc Jodoin, *The Representation Theory of Neural Networks*, arXiv:2007.12213 (2020). [↑1, 3](#)

- [AJP⁺21] Marco Armenta, Thierry Judge, Nathan Painchaud, Youssef Skandarani, Carl Lemaire, Gabriel Gibeau Sanchez, Philippe Spino, and Pierre-Marc Jodoin, *Neural Teleportation*, arXiv:2012.01118 [cs] (August 2021). arXiv: 2012.01118. [↑1, 3](#)
- [BC13] Lei Jimmy Ba and Rich Caruana, *Do deep nets really need to be deep?*, arXiv:1312.6184 (2013). [↑4](#)
- [BCNM06] Cristian Buciluă, Rich Caruana, and Alexandru Niculescu-Mizil, *Model compression*, Proceedings of the 12th ACM SIGKDD International Conference on Knowledge Discovery and Data Mining, 2006, pp. 535–541. [↑4](#)
- [BL88] David S Broomhead and David Lowe, *Radial basis functions, multi-variable functional interpolation and adaptive networks*, Royal Signals and Radar Establishment Malvern (United Kingdom), 1988. [↑4](#)
- [BOFG20] Davis Blalock, Jose Javier Gonzalez Ortiz, Jonathan Frankle, and John Gutttag, *What is the state of neural network pruning?*, arXiv:2003.03033 (2020). [↑4](#)
- [BS19] Erkao Bao and Linqi Song, *Equivariant neural networks and equivarification*, arXiv:1906.07172 (2019). [↑4](#)
- [CDM18] Benjamin Chidester, Minh N. Do, and Jian Ma, *Rotation equivariance and invariance in convolutional neural networks*, arXiv:1805.12301 (2018). [↑4](#)
- [CFF⁺15] Yu Cheng, X Yu Felix, Rogerio S Feris, Sanjiv Kumar, Alok Choudhary, and Shih-Fu Chang, *Fast neural networks with circulant projections*, arXiv:1502.03436 2 (2015). [↑4](#)
- [CW16] Taco S. Cohen and Max Welling, *Group equivariant convolutional networks*, International conference on machine learning (ICML), 2016, pp. 2990–2999. [↑1, 4](#)
- [CW17] Taco S Cohen and Max Welling, *Steerable CNNs*, Proceedings of the International Conference on Learning Representations (ICLR), 2017. [↑1, 4](#)
- [CWKW19] Taco S. Cohen, Maurice Weiler, Berkay Kicanaoglu, and Max Welling, *Gauge equivariant convolutional networks and the icosahedral CNN*, Proceedings of the 36th International Conference on Machine Learning (ICML), 2019, pp. 1321–1330. [↑4](#)
- [CWZZ17] Yu Cheng, Duo Wang, Pan Zhou, and Tao Zhang, *A survey of model compression and acceleration for deep neural networks*, arXiv:1710.09282 (2017). [↑4](#)
- [CYF⁺15] Yu Cheng, Felix X Yu, Rogerio S Feris, Sanjiv Kumar, Alok Choudhary, and Shi-Fu Chang, *An exploration of parameter redundancy in deep networks with circulant projections*, Proceedings of the IEEE International Conference on Computer Vision, 2015, pp. 2857–2865. [↑4](#)
- [DCP17] Xin Dong, Shangyu Chen, and Sinno Jialin Pan, *Learning to prune deep neural networks via layer-wise optimal brain surgeon*, arXiv preprint arXiv:1705.07565 (2017). [↑4](#)
- [DFK16] Sander Dieleman, Jeffrey De Fauw, and Koray Kavukcuoglu, *Exploiting cyclic symmetry in convolutional neural networks*, International Conference on Machine Learning (ICML), 2016. [↑4](#)
- [DLD⁺21] Congyue Deng, O. Litany, Yueqi Duan, A. Poulernard, A. Tagliasacchi, and L. Guibas, *Vector Neurons: A General Framework for SO(3)-Equivariant Networks*, 2021 IEEE/CVF International Conference on Computer Vision (ICCV) (2021). [↑4](#)
- [DPBB17] Laurent Dinh, Razvan Pascanu, Samy Bengio, and Yoshua Bengio, *Sharp Minima Can Generalize For Deep Nets*, International Conference on Machine Learning (ICML), July 2017, pp. 1019–1028. [↑3, 10](#)
- [FC18] Jonathan Frankle and Michael Carbin, *The lottery ticket hypothesis: Finding sparse, trainable neural networks*, arXiv:1803.03635 (2018). [↑4](#)
- [FSIW20] Marc Finzi, Samuel Stanton, Pavel Izmailov, and Andrew Gordon Wilson, *Generalizing convolutional networks for equivariance to lie groups on arbitrary continuous data.*, Proceedings of the international conference on machine vision and machine learning, 2020. [↑4](#)
- [GLYB14] Yunchao Gong, Liu Liu, Ming Yang, and Lubomir Bourdev, *Compressing deep convolutional networks using vector quantization*, arXiv:1412.6115 (2014). [↑4](#)
- [GvLW22] Iordan Ganev, Twan van Laarhoven, and Robin Walters, *Universal approximation and model compression for radial neural networks*, arXiv, 2022. Number: arXiv:2107.02550 arXiv:2107.02550 [cs, math]. [↑2, 3, 4, 7, 9, 24, 27](#)
- [HLVDMW17] Gao Huang, Zhuang Liu, Laurens Van Der Maaten, and Kilian Q. Weinberger, *Densely Connected Convolutional Networks*, 2017 IEEE Conference on Computer Vision and Pattern Recognition (CVPR), July 2017, pp. 2261–2269. ISSN: 1063-6919. [↑2](#)
- [HMD15] Song Han, Huizi Mao, and William J Dally, *Deep compression: Compressing deep neural networks with pruning, trained quantization and Huffman coding*, arXiv:1510.00149 (2015). [↑4](#)
- [HS93] Babak Hassibi and David G Stork, *Second order derivatives for network pruning: Optimal brain surgeon*, Morgan Kaufmann, 1993. [↑4](#)
- [HVD15] Geoffrey Hinton, Oriol Vinyals, and Jeff Dean, *Distilling the knowledge in a neural network*, arXiv:1503.02531 (2015). [↑4](#)

- [HZC⁺17] Andrew G Howard, Menglong Zhu, Bo Chen, Dmitry Kalenichenko, Weijun Wang, Tobias Weyand, Marco Andreetto, and Hartwig Adam, *MobileNets: Efficient convolutional neural networks for mobile vision applications*, arXiv:1704.04861 (2017). [↑4](#)
- [JL21] George Jeffreys and Siu-Cheong Lau, *Kähler Geometry of Quiver Varieties and Machine Learning*, arXiv:2101.11487 (2021). [↑1, 3, 4](#)
- [Kar90] Ehud D Karnin, *A simple procedure for pruning back-propagation trained neural networks*, IEEE transactions on neural networks **1** (1990), no. 2, 239–242. [↑4](#)
- [KJ16] Alexander Kirillov Jr, *Quiver representations and quiver varieties*, Vol. 174, American Mathematical Soc., 2016. [↑1](#)
- [KT18] Risi Kondor and Shubhendu Trivedi, *On the Generalization of Equivariance and Convolution in Neural Networks to the Action of Compact Groups*, International conference on machine learning (ICML), 2018. [↑1, 4](#)
- [KW16] Thomas N Kipf and Max Welling, *Semi-supervised classification with graph convolutional networks*, arXiv preprint arXiv:1609.02907 (2016). [↑3](#)
- [LAGT19] Namhoon Lee, Thalaiyasingam Ajanthan, Stephen Gould, and Philip HS Torr, *A signal propagation perspective for pruning neural networks at initialization*, arXiv preprint arXiv:1906.06307 (2019). [↑4](#)
- [LDS90] Yann LeCun, John S Denker, and Sara A Solla, *Optimal brain damage*, Advances in neural information processing systems, 1990, pp. 598–605. [↑4](#)
- [LGR⁺14] Vadim Lebedev, Yaroslav Ganin, Maksim Rakhuba, Ivan Oseledets, and Victor Lempitsky, *Speeding-up convolutional neural networks using fine-tuned cp-decomposition*, arXiv:1412.6553 (2014). [↑4](#)
- [LKZ⁺17] Yongxi Lu, Abhishek Kumar, Shuangfei Zhai, Yu Cheng, Tara Javidi, and Rogerio Feris, *Fully-adaptive feature sharing in multi-task networks with applications in person attribute classification*, Proceedings of the IEEE conference on computer vision and pattern recognition (CVPR), 2017, pp. 5334–5343. [↑4](#)
- [LW21] Leon Lang and Maurice Weiler, *A Wigner-Eckart theorem for group equivariant convolution kernels*, International conference on learning representations (ICLR), 2021. [↑4](#)
- [MM20] Yuri Manin and Matilde Marcolli, *Homotopy Theoretic and Categorical Models of Neural Information Networks*, arXiv:2006.15136 (2020). [↑3](#)
- [MTK⁺16] Pavlo Molchanov, Stephen Tyree, Tero Karras, Timo Aila, and Jan Kautz, *Pruning convolutional neural networks for resource efficient inference*, arXiv preprint arXiv:1611.06440 (2016). [↑4](#)
- [MYF⁺18] Ahmed Mohammed, Sule Yildirim, Ivar Farup, Marius Pedersen, and Oistein Hovde, *Y-Net: A deep Convolutional Neural Network for Polyp Detection*, arXiv, 2018. Number: arXiv:1806.01907 arXiv:1806.01907 [cs]. [↑2, 6](#)
- [MZZ⁺19] Qi Meng, Shuxin Zheng, Huishuai Zhang, Wei Chen, Qiwei Ye, Zhi-Ming Ma, Nenghai Yu, and Tie-Yan Liu, *G-SGD: Optimizing ReLU Neural Networks in its Positively Scale-Invariant Space* (2019). [↑3, 10](#)
- [NSS15] Behnam Neyshabur, Ruslan Salakhutdinov, and Nathan Srebro, *Path-SGD: path-normalized optimization in deep neural networks*, Proceedings of the 28th International Conference on Neural Information Processing Systems - Volume 2, December 2015, pp. 2422–2430. [↑3, 10](#)
- [N⁺98] Hiraku Nakajima et al., *Quiver varieties and Kac-Moody algebras*, Duke Mathematical Journal **91** (1998), no. 3, 515–560. [↑1](#)
- [PMR] Alejandro Parada-Mayorga and Alejandro Ribeiro, *Algebraic Neural Networks: Stability to Deformations*, arXiv:2009.01433v3. [↑3](#)
- [RSLF13] Roberto Rigamonti, Amos Sironi, Vincent Lepetit, and Pascal Fua, *Learning separable filters*, Proceedings of the IEEE conference on computer vision and pattern recognition, 2013, pp. 2754–2761. [↑4](#)
- [RSP17] Siamak Ravanbakhsh, Jeff Schneider, and Barnabas Poczos, *Equivariance through parameter-sharing*, International Conference on Machine Learning, 2017, pp. 2892–2901. [↑1, 4](#)
- [SFH17] Sara Sabour, Nicholas Frosst, and Geoffrey E Hinton, *Dynamic routing between capsules*, arXiv:1710.09829 (2017). [↑3](#)
- [SKR20] Thiago Serra, Abhinav Kumar, and Srikumar Ramalingam, *Lossless compression of deep neural networks*, International conference on integration of constraint programming, artificial intelligence, and operations research, 2020, pp. 417–430. [↑4](#)
- [SLD17] Evan Shelhamer, Jonathan Long, and Trevor Darrell, *Fully Convolutional Networks for Semantic Segmentation*, IEEE transactions on pattern analysis and machine intelligence **39** (April 2017), no. 4, 640–651 (eng). [↑2, 6](#)
- [SYKR21] Thiago Serra, Xin Yu, Abhinav Kumar, and Srikumar Ramalingam, *Scaling up exact neural network compression by relu stability*, Advances in Neural Information Processing Systems **34** (2021). [↑4](#)

- [SZK20] Gustav Sourek, Filip Zelezny, and Ondrej Kuzelka, *Lossless compression of structured convolutional models via lifting*, arXiv preprint arXiv:2007.06567 (2020). [↑4](#)
- [TXZ⁺15] Cheng Tai, Tong Xiao, Yi Zhang, Xiaogang Wang, et al., *Convolutional neural networks with low-rank regularization*, arXiv:1511.06067 (2015). [↑4](#)
- [WC19] Maurice Weiler and Gabriele Cesa, *General $E(2)$ -Equivariant Steerable CNNs*, Conference on Neural Information Processing Systems (NeurIPS) (2019). [↑3, 4, 9](#)
- [WGTB17] Daniel E Worrall, Stephan J Garbin, Daniyar Turmukhambetov, and Gabriel J Brostow, *Harmonic networks: Deep translation and rotation equivariance*, Proceedings of the IEEE Conference on Computer Vision and Pattern Recognition (CVPR), 2017, pp. 5028–5037. [↑4](#)
- [WGW⁺18] Maurice Weiler, Mario Geiger, Max Welling, Wouter Boomsma, and Taco Cohen, *3D steerable CNNs: Learning rotationally equivariant features in volumetric data*, Proceedings of the 32nd International Conference on Neural Information Processing Systems (NeurIPS) (2018). [↑3](#)
- [WHS18] Maurice Weiler, Fred A Hamprecht, and Martin Storath, *Learning steerable filters for rotation equivariant CNNs*, Proceedings of the IEEE Conference on Computer Vision and Pattern Recognition (CVPR), 2018, pp. 849–858. [↑3, 4](#)
- [WLW⁺16] Jiaxiang Wu, Cong Leng, Yuhang Wang, Qinghao Hu, and Jian Cheng, *Quantized convolutional neural networks for mobile devices*, Proceedings of the IEEE conference on computer vision and pattern recognition (CVPR), 2016, pp. 4820–4828. [↑4](#)
- [WST96] Jeffrey Wood and John Shawe-Taylor, *Representation theory and invariant neural networks*, Discrete Applied Mathematics **69** (August 1996), no. 1, 33–60. [↑3](#)
- [WZG20] Chaoqi Wang, Guodong Zhang, and Roger Grosse, *Picking winning tickets before training by preserving gradient flow*, arXiv preprint arXiv:2002.07376 (2020). [↑4](#)
- [ZSKS17] Julian Georg Zilly, Rupesh Kumar Srivastava, Jan Koutník, and Jürgen Schmidhuber, *Recurrent Highway Networks*, Proceedings of the 34th International Conference on Machine Learning - Volume 70, August 2017, pp. 4189–4198. [↑2](#)

APPENDIX A. MODEL COMPRESSION

In this appendix, we discuss model compression in more detail. We begin with a proof of Theorem 4.1, elaborate on an improvement and an alternative to Algorithm 1, define subnetworks of quiver neural networks, and include results about radial neural networks.

A.1. Proof of Theorem 4.1. We adopt the notation of Section 4 and Algorithm 1. For each vertex i , let $\lambda_i : \mathbb{R}^{d_i} \rightarrow \mathbb{R}$ be the rescaling factor for the rescaling activation ρ_i .

Lemma A.1. *For any vertex i :*

- (1) *The function τ_i is a rescaling activation with rescaling factor equal to $\lambda_i \circ Q_i \circ \text{Inc}_i$.*
- (2) *The following identity holds: $Q_i \circ \text{Inc}_i \circ \tau_i = \rho_i \circ Q_i \circ \text{Inc}_i$.*

Proof. Let $x \in \mathbb{R}^{d_i^{\text{red}}}$. To show the first claim, we compute:

$$\begin{aligned} \tau_i(x) &= \pi_i \circ Q_i^{-1} \circ \rho_i \circ Q_i \circ \text{Inc}_i(x) = \pi_i \circ Q_i^{-1} (\lambda_i(Q_i \circ \text{Inc}_i(x)) Q_i \circ \text{Inc}_i(x)) \\ &= \pi_i (\lambda_i(Q_i \circ \text{Inc}_i(x)) \text{Inc}_i(x)) = \lambda_i(Q_i \circ \text{Inc}_i(x)) x \end{aligned}$$

where we use the fact that Q_i is a linear map, and that the composition $\pi_i \circ \text{Inc}_i$ is the identity on $\mathbb{R}^{d_i^{\text{red}}}$. This proves the first claim. For the second claim, we compute:

$$Q_i \circ \text{Inc}_i \circ \tau_i(x) = Q_i \circ \text{Inc}_i (\lambda_i(Q_i \circ \text{Inc}_i(x)) x) = \lambda_i(Q_i \circ \text{Inc}_i(x)) (Q_i \circ \text{Inc}_i(x)) = \rho_i \circ Q_i \circ \text{Inc}_i(x)$$

where we use the fact that Q_i and Inc_i are linear maps. \square

We require some notation for the remainder of the proof. Let F be the feedforward function of the input network $(\mathbf{d}, \mathbf{W}, \rho)$ and F^{red} the feedforward function of the compressed network $(\mathbf{d}^{\text{red}}, \mathbf{W}^{\text{red}}, \tau)$ produced by Algorithm 1. Correspondingly, we have the partial feedforward functions F_i and F_i^{red} for every vertex i . Set $d_{\rightarrow i}^{\text{red}} = \sum_{e \in t^{-1}(i)} d_{s(e)}^{\text{red}}$ to be the sum of the reduced dimension vector values d_j^{red} for vertices j with an outgoing edge to vertex i . Enumerate the incoming edges as $e_1, \dots, e_{|t^{-1}(i)|}$. Let M_i be as in the algorithm, so that:

$$M_i = \left[W_{e_1} \circ Q_{s(e_1)} \circ \text{Inc}_{s(e_1)} \quad \cdots \quad W_{e_{|t^{-1}(i)|}} \circ Q_{s(e_{|t^{-1}(i)|})} \circ \text{Inc}_{s(e_{|t^{-1}(i)|})} \right] \in \mathbb{R}^{d_i \times d_{\rightarrow i}}$$

For $x \in \mathbb{R}^{d_{\text{in}}}$, set

$$F_{\rightarrow i}^{\text{red}}(x) = \begin{bmatrix} F_{s(e_1)}^{\text{red}}(x) \\ \vdots \\ F_{s(e_{|t^{-1}(i)|})}^{\text{red}}(x) \end{bmatrix} \in \mathbb{R}^{d_{\rightarrow i}}.$$

Next, we show that:

$$(A.1) \quad F_i = Q_i \circ \text{Inc}_i \circ F_i^{\text{red}}$$

for all vertices i , where $Q_i = \text{Id}_{d_i}$ if i is a source or sink. We proceed by induction. The base case is when i is a source, and is easy. For the induction step, we take $x \in \mathbb{R}^{d_{\text{in}}}$ and compute:

$$\begin{aligned} F_i(x) &= \rho_i \left(\sum_{e \in t^{-1}(i)} W_e \circ F_{s(e)}(x) \right) = \rho_i \left(\sum_{e \in t^{-1}(i)} W_e \circ Q_{s(e)} \circ \text{Inc}_{s(e)} \circ F_{s(e)}^{\text{red}}(x) \right) = \rho_i \circ M_i \circ F_{\rightarrow i}^{\text{red}}(x) \\ &= \rho_i \circ Q_i \circ \text{Inc}_i \circ R_i \circ F_{\rightarrow i}^{\text{red}}(x) = Q_i \circ \text{Inc}_i \circ \tau_i \circ R_i \circ F_{\rightarrow i}^{\text{red}}(x) \\ &= Q_i \circ \text{Inc}_i \circ \tau_i \left(\sum_{e \in t^{-1}(i)} W_e^{\text{red}} \circ F_{s(e)}^{\text{red}}(x) \right) = Q_i \circ \text{Inc}_i \circ F_i^{\text{red}}(x) \end{aligned}$$

where the first equality follows from the definition of F_i ; the second from the induction hypothesis; the third from the definitions of M_i and $F_{\rightarrow i}^{\text{red}}(x)$; the fourth from the definitions of Q_i and R_i ; the fifth from the Lemma A.1; the sixth from the definition of R_e and $F_{\rightarrow i}^{\text{red}}(x)$; and the last from the definition of F_i^{red} . This establishes Equation A.1. The theorem now follows from the definition of the feedforward function, and the fact that $Q_i = \text{Inc}_i = \text{Id}_{d_i}$ if i is a sink.

A.2. Improvement to Algorithm 1. As mentioned in Section 4, our model compression algorithm can be improved by considering the ranks of the matrices M_i . We give this improvement in Algorithm 2, displayed at the end of this appendix. For clarity, we describe the algorithm in more detail as follows. Set $k_i = d_i$ for each source and sink vertex i . Fix a topological order of the vertices, and, for each vertex that is neither a source nor a sink, do:

- (1) Define \tilde{M}_i using a merging procedure as before, except use the inclusion map $\text{Inc}_{k_i, d_i} : \mathbb{R}^{k_i} \hookrightarrow \mathbb{R}^{d_i}$ into the first k_i coordinates instead of $\text{Inc}_{d_i^{\text{red}}, d_i}$. So \tilde{M}_i is of size $d_i \times k_{\rightarrow i}$. We abbreviate Inc_{k_i, d_i} by $\tilde{\text{Inc}}_i$.
- (2) Let k_i be the rank of \tilde{M}_i . Observe that $k_i \leq \min(d_i, k_{\rightarrow i})$, so $k_i \leq d_i^{\text{red}}$.
- (3) Set $P_i \in \mathbb{R}^{k_{\rightarrow i} \times k_{\rightarrow i}}$ to be a permutation matrix such that the first k_i columns of \tilde{M}_i are linearly independent.
- (4) Let $\tilde{Q}_i \tilde{\text{Inc}}_i \tilde{R}_i$ be the complete QR decomposition of $\tilde{M}_i P_i$. Note that the choice of permutation P_i implies that \tilde{R}_i is full rank.
- (5) Set $\tilde{W}_{\rightarrow i}^{\text{red}} = \tilde{R}_i P_i^{-1}$, which is a full-rank matrix of size $k_i \times k_{\rightarrow i}$. Since $k_i \leq k_{\rightarrow i}$, we see that in fact $\tilde{W}_{\rightarrow i}^{\text{red}}$ is surjective.
- (6) Extract the matrices \tilde{W}_e^{red} from $\tilde{W}_{\rightarrow i}^{\text{red}}$ as in the original algorithm.
- (7) Update the activation ρ_i to $\tilde{\tau}_i = \tilde{\pi}_i \circ \tilde{Q}_i^{-1} \circ \rho_i \circ \tilde{Q}_i \circ \tilde{\text{Inc}}_i$ where $\tilde{\pi}_i : \mathbb{R}^{d_i} \rightarrow \mathbb{R}^{k_i}$ is the projection onto the first k_i coordinates.

For sink vertices, one updates the weight matrix W_e on each incoming edge to $W_e \circ \tilde{Q}_{s(e)} \circ \tilde{\text{Inc}}_{s(e)}$. Using this version of the algorithm, the compressed network has dimension vector $\mathbf{k} = (k_i)$. The methods `hstack`, `rank`, `permutation`, and `extract` of Algorithm 2 reflect the procedures described in steps (1), (2), (3), and (6) above, respectively.

Observe that Algorithm 2 provides an actual improvement only if some of the matrices \tilde{M}_i matrices are not of full rank (otherwise $k_i = d_i^{\text{red}}$ for all vertices i), which is a situation uncommon in practical applications. One can also replace each \tilde{M}_i by a version with singular values above a given threshold. In this case, the feedforward function of the compressed model would differ from that of the original model, so the compression would not be lossless.

Examination of Algorithm 2 reveals that the image of the common feedforward functions of the compressed and original models lies in a subspace of $\mathbb{R}^{k_{\text{out}}} = \mathbb{R}^{d_{\text{out}}}$ of dimension $\sum_{i \in \text{sinks}} \text{rank}(\tilde{M}_i)$, where \tilde{M}_i is defined in the same way for sinks as it is for non-sinks. Hence, if desired, the basis of the output space can be changed to make k_i equal to $\text{rank}(\tilde{M}_i)$ for output vertices. Similar remarks hold for Algorithm 1, where $d_i^{\text{red}} = \min(d_i, d_{\rightarrow i}^{\text{red}})$ for output vertices if one allows changes of basis for the output space.

A.3. Alternative algorithm. A key tool in Algorithm 1 is the use of the QR decomposition to effectively change the basis of the feature spaces \mathbb{R}^{d_i} at the hidden vertices. It is possible to preform this change-of-basis differently, as exhibited in Algorithm 3 (displayed at the end of this appendix). For clarity, we describe the algorithm in more detail as follows. For every source vertex, set B_i to be the identity $d_i \times d_i$ matrix and set $k_i = d_i$. For each vertex that is neither a source nor a sink, do:

- (1) Form the matrix \hat{B}_i to be the $d_i \times k_{\rightarrow i}$ matrix formed by horizontally concatenating the matrices $W_e B_{s(e)}$ for all incoming edges to i .
- (2) Proceeding from left to right, check if each column of \hat{B}_i is in the span of the preceding columns, and if so, remove it.
- (3) Set k_i to be the number of columns of B_i . (Equivalently, k_i is the rank of \hat{B}_i .)
- (4) Observe that B_i is injective, so there exists a matrix C_i such that $C_i B_i$ is the identity $k_i \times k_i$ matrix. We call C_i a left inverse of B_i , and note that it is not unique in general. An adequate choice can be easily computed.
- (5) Set $\tilde{\tau}_i$ to be $C_i \circ \rho_i \circ B_i$.
- (6) For each incoming edge e to i , set \tilde{W}_e^{red} to be the matrix product $C_i W_e B_{s(e)}$, which is a matrix of size $k_i \times k_{s(e)}$.

For sink vertices, one sets $k_i = d_i$ and updates the weight matrix W_e on each incoming edge to $W_e \circ B_{s(e)}$. The methods `hstack`, `full_rank`, `num_col`, and `left_inverse` of Algorithm 3 reflect the procedures described in steps (1), (2), (3), and (4) above, respectively. It is easy to verify that, for any vertex i and any edge $j \xrightarrow{e} i$, we have $B_i \circ \tau_i = \rho_i \circ B_i$ and $B_i \circ W_e^{\text{red}} = W_e \circ B_j$, where we use the notation of Algorithm 3. Furthermore, we recover the model compression of Algorithm 3 from Algorithm 2 by setting $B_i := \tilde{Q}_i \circ \text{In}_i$, $C_i = \tilde{\pi}_i \circ \tilde{Q}_i^{-1}$, and $\tau_i = \tilde{\pi}_i \circ \tilde{Q}_i^{-1} \circ \rho_i \circ \tilde{Q}_i \circ \text{In}_i$.

A.4. Subnetworks of quiver neural networks. We now introduce the notation of a subnetwork of a \mathcal{Q} -neural network, and prove that the feedforward function of a subnetwork is intertwined with the feedforward function of the full network. Algorithms 1, 2, and 3 each produce a subnetwork of the original input \mathcal{Q} -neural network. In the case of Algorithms 2 and 3, the subnetworks are minimal in certain precise sense that we explain below.

Let \mathcal{Q} be a neural quiver. A *subnetwork* of a \mathcal{Q} -neural network $(\mathbf{d}, \mathbf{W}, \rho)$ consists of a \mathcal{Q} -neural network $(\mathbf{k}, \mathbf{V}, \tau)$ together with an injective linear map $\alpha_i : \mathbb{R}^{k_i} \hookrightarrow \mathbb{R}^{d_i}$ for each vertex such that:

$$W_e \circ \alpha_{s(e)} = V_e \circ \alpha_{t(e)} \quad \text{and} \quad \rho_i \circ \alpha_i = \alpha_i \circ \tau_i$$

for each vertex i and each edge e , and $\alpha_{i_{\text{bias}}}$ is the identity for the bias vertex. We group the maps α_i into a tuple $\alpha = (\alpha_i)$ and write $(\mathbf{k}, \mathbf{V}, \tau) \xrightarrow{\alpha} (\mathbf{d}, \mathbf{W}, \rho)$. We see that $k_i \leq d_i$ for each vertex i . The maps α_i define maps $\alpha_{\text{in}} : \mathbb{R}^{k_{\text{in}}} \hookrightarrow \mathbb{R}^{d_{\text{in}}}$ and $\alpha_{\text{out}} : \mathbb{R}^{k_{\text{out}}} \hookrightarrow \mathbb{R}^{d_{\text{out}}}$.

Proposition A.2. Let $(\mathbf{k}, \mathbf{V}, \tau) \xrightarrow{\alpha} (\mathbf{d}, \mathbf{W}, \rho)$ be a subnetwork, and let \tilde{F} and F be the respective feedforward functions. Then:

$$F \circ \alpha_{\text{in}} = \alpha_{\text{out}} \circ \tilde{F}$$

Sketch of proof. It suffices to show that the partial feedforward functions satisfy $F_i \circ \alpha_{\text{in}} = \alpha_i \circ \tilde{F}_i$ for all vertices i . To this end, we fix a topological order and proceed by induction. The base step is straightforward (using the fact that $\alpha_{i_{\text{bias}}} = \text{Id}_{\mathbb{R}}$). The key computation in the induction step is:

$$\begin{aligned} F_i \circ \alpha_{\text{in}} &= \rho_i \left(\sum_{e \in t^{-1}(i)} W_e \circ F_{s(e)} \circ \alpha_{\text{in}} \right) = \rho_i \left(\sum_{e \in t^{-1}(i)} W_e \circ \alpha_i \circ \tilde{F}_{s(e)} \right) = \rho_i \left(\sum_{e \in t^{-1}(i)} \alpha_i \circ V_{s(e)} \circ \tilde{F}_{s(e)} \right) \\ &= \rho_i \circ \alpha_i \left(\sum_{e \in t^{-1}(i)} V_{s(e)} \circ \tilde{F}_{s(e)} \right) = \alpha_i \circ \tau_i \left(\sum_{e \in t^{-1}(i)} V_{s(e)} \circ \tilde{F}_{s(e)} \right) = \alpha_i \circ \tilde{F}_i \end{aligned}$$

□

Proposition A.3. The outputs of Algorithms 1, 2, and 3 each produce a subnetwork of the original input \mathcal{Q} -neural network with rescaling activations.

We omit a full proof of this proposition, as it is straightforward: one uses the maps $\alpha_i = Q_i \text{Inc}_i$, $\alpha_i = \tilde{Q}_i \tilde{\text{Inc}}_i$, and $\alpha_i = B_i$, respectively. Note that we recover Theorem 4.1 from Propositions A.2 and A.3 since $Q_i \text{Inc}_i$ is the identity for any source or sink.

We say that a subnetwork $(\mathbf{k}, \mathbf{V}, \tau) \xrightarrow{\alpha} (\mathbf{d}, \mathbf{W}, \rho)$ is *source-framed* if we have $k_i = d_i$ and $\alpha_i = \text{Id}_{d_i}$ for any source vertex i . We say that a subnetwork of a \mathcal{Q} -neural network $(\mathbf{d}, \mathbf{W}, \rho)$ is *minimal* if the following two conditions are satisfied: (1) it is source-framed, and (2) it a subnetwork of any other source-framed subnetwork of $(\mathbf{d}, \mathbf{W}, \rho)$. In particular, the value of the dimension vector of any other subnetwork is at least k_i at each vertex i .

Proposition A.4. The outputs of Algorithms 2 and 3 each produce the minimal subnetwork of the original input \mathcal{Q} -neural network with rescaling activations.

Proof. We give a proof only in the case of Algorithm 2; the argument for Algorithm 3 is similar.

Set $\alpha_i = \tilde{Q}_i \tilde{\text{Inc}}_i$. Suppose $(\mathbf{n}, \mathbf{U}, \nu) \xrightarrow{\beta} (\mathbf{d}, \mathbf{W}, \rho)$ is a source-framed subnetwork. For each vertex, we aim to define an injective linear map

$$\psi_i : \mathbb{R}^{k_i} \rightarrow \mathbb{R}^{n_i}$$

such that $\beta_i \circ \psi_i = \alpha_i$. If i is a source, set ψ_i to be the identity. Proceeding by induction over a topological order of the vertices, take a non-source vertex i and assume that we have defined ψ_j for all vertices j with an outgoing edge to i . For a fixed ordering of the edges, we form the matrix $W_{\rightarrow i} \in \mathbb{R}^{d_i \times d_{\rightarrow i}}$ by horizontally stacking the matrices W_e for edges incoming to i . Similarly we have the matrices $U_{\rightarrow i} \in \mathbb{R}^{n_i \times n_{\rightarrow i}}$ and $\tilde{W}_{\rightarrow i}^{\text{red}} \in \mathbb{R}^{k_i \times k_{\rightarrow i}}$. We also have the linear map $\alpha_{\rightarrow i} : \bigoplus_{j \rightarrow i} \mathbb{R}^{k_j} \rightarrow \bigoplus_{j \rightarrow i} \mathbb{R}^{d_j}$, defined as $\alpha_{\rightarrow i} = \bigoplus_{j \rightarrow i} \alpha_j$. The maps $\beta_{\rightarrow i}$ and $\psi_{\rightarrow i}$ are defined analogously. We compute:

$$\alpha_i \circ \tilde{W}_{\rightarrow i}^{\text{red}} = W_{\rightarrow i} \circ \alpha_{\rightarrow i} = W_{\rightarrow i} \circ \beta_{\rightarrow i} \circ \psi_{\rightarrow i} = \beta_{\rightarrow i} \circ U_{\rightarrow i} \circ \psi_{\rightarrow i}$$

where the first equality uses the fact that the α_j define subnetwork, the second equality uses the induction hypothesis, and the third uses the fact that the β_j define a subnetwork. Recall from

the discussion in Section A.2 that the matrix $\tilde{W}_{\rightarrow i}^{\text{red}}$ is surjective. It follows that the image of α_i is contained in the image of β_i . Hence, we can choose a map $\psi_i : \mathbb{R}^{k_i} \rightarrow \mathbb{R}^{n_i}$ such that $\beta_i \circ \psi_i = \alpha_i$. Since α_i is injective, so is ψ_i .

Now that the maps ψ_i have been defined, it is straightforward to show that $\psi_{t(e)} \circ \tilde{W}_e^{\text{red}} \circ \psi_{s(e)}$ for any edge e , and that $\psi_i \circ \tau_i = \nu_i \circ \psi_i$ for any vertex i . Thus, $(\mathbf{k}, \tilde{\mathbf{W}}^{\text{red}}, \boldsymbol{\tau})$ is a subnetwork of $(\mathbf{n}, \mathbf{U}, \boldsymbol{\nu})$ via the maps ψ_i . \square

A.5. Radial rescaling functions. In this section, we turn our attention to radial rescaling activations and radial neural networks. We first prove the following basic fact about radial rescaling functions:

Lemma A.5. *A rescaling function commutes with orthogonal transformations if and only if it is a radial rescaling function.*

Proof. It is straightforward to show that any radial rescaling function commutes with orthogonal transformations. For the opposite direction, suppose ρ is a rescaling activation on \mathbb{R}^d with rescaling scalar-valued function $\lambda : \mathbb{R}^d \rightarrow \mathbb{R}$, and suppose ρ commutes with orthogonal transformations. Then, one easily shows that $\lambda(Qv) = \lambda(v)$ for any $v \in \mathbb{R}^d$ and any $Q \in O(d)$. Since any two elements of \mathbb{R}^d of the same norm are related by an orthogonal transformation, it follows that the rescaling factor $\lambda(v)$ depends only on the norm of v . \square

Next, we restate and prove Proposition 4.2.

Proposition 4.2. *For radial \mathcal{Q} -neural networks, Algorithm 1 leaves the activation functions unchanged.*

Proof. The fact that each activation ρ_i commutes with orthogonal transformations implies that $Q_i^{-1} \circ \rho_i \circ Q_i = \rho_i$. Hence, in Algorithm 1, we have $\tau_i \leftarrow \pi_i \circ \rho_i \circ \text{Inc}_i$ for any hidden vertex i . The image of $\mathbb{R}^{d_i^{\text{red}}}$ under ρ_i lies in $\mathbb{R}^{d_i^{\text{red}}}$, so τ_i is nothing more than the restriction of ρ_i to $\mathbb{R}^{d_i^{\text{red}}}$. \square

Finally, we consider subnetworks of radial \mathcal{Q} -neural networks. Let \mathcal{Q} be a neural quiver. A *radial subnetwork* of a radial \mathcal{Q} -neural network $(\mathbf{d}, \mathbf{W}, \boldsymbol{\rho})$ consists of a radial \mathcal{Q} -neural network $(\mathbf{k}, \mathbf{V}, \boldsymbol{\tau})$ together with a linear isometry $\alpha_i : \mathbb{R}^{k_i} \hookrightarrow \mathbb{R}^{d_i}$ for each vertex such that: $W_e \circ \alpha_{s(e)} = V_e \circ \alpha_{t(e)}$ and $\rho_i \circ \alpha_i = \alpha_i \circ \tau_i$ for each vertex i and each edge e . Recall that the condition for α_i to be an isometry is that it is norm-preserving: $|\alpha_i(x)| = |x|$ for each $x \in \mathbb{R}^{k_i}$. Note that any linear isometry is injective. The analogues of Propositions A.3 and A.4 hold for radial rescaling activations, and are proven in essentially the same way.

Algorithm 2: Improved model compression for rescaling activations (see Section A.2)

```

input   :  $\mathcal{Q}$ -neural network  $(\mathbf{d}, \mathbf{W}, \rho)$  with each  $\rho_i$  rescaling
output  :  $\mathcal{Q}$ -neural network  $(\mathbf{k}, \tilde{\mathbf{W}}^{\text{red}}, \tilde{\tau})$ , orthogonal matrices  $\tilde{\mathbf{Q}} = (Q_i \in O(d_i))_{i \in I_{\text{hidden}}}$ 
for  $i$  in  $I$  do                                     // vertices are in topological order
    if  $i$  is not a source or sink then
         $\tilde{M}_i \leftarrow \text{hstack}(W_e Q_{s(e)} \tilde{\text{Inc}}_{s(e)} : t(e) = i)$            // concatenate matrices
         $k_i \leftarrow \text{rank}(\tilde{M}_i)$ 
         $P_i \leftarrow \text{permutation}(\tilde{M}_i, k_i)$                                // permutation matrix
         $\tilde{Q}_i, \tilde{R}_i \leftarrow \text{QR-decomp}(\tilde{M}_i P_i, \text{mode} = \text{'complete'})$        //  $M_i P_i = \tilde{Q}_i \tilde{\text{Inc}}_i \tilde{R}_i$ 
        for  $e$  such that  $t(e) = i$  do
             $\tilde{W}_e^{\text{red}} \leftarrow \text{extract}(\tilde{R}_i P_i^{-1}, e)$                  // extract the reduced weights
        end
         $\tilde{\tau}_i \leftarrow \tilde{\tau}_i \circ \tilde{Q}_i^{-1} \circ \rho_i \circ \tilde{Q}_i \circ \tilde{\text{Inc}}_i$        // update the activations
    else if  $i$  is a sink then
         $\tilde{\tau}_i \leftarrow \rho_i$ 
        for  $e$  such that  $t(e) = i$  do
             $\tilde{W}_e^{\text{red}} \leftarrow W_e \tilde{Q}_{s(e)} \tilde{\text{Inc}}_{s(e)}$                  // extract the reduced weights
        end
end
return  $(\mathbf{k}, \tilde{\mathbf{W}}^{\text{red}}, \tilde{\tau})$ , and  $\tilde{\mathbf{Q}}$ 
    
```

Algorithm 3: Alternative model compression for rescaling activations (see Section A.3)

```

input   :  $\mathcal{Q}$ -neural network  $(\mathbf{d}, \mathbf{W}, \rho)$  with each  $\rho_i$  rescaling
output  :  $\mathcal{Q}$ -neural network  $(\mathbf{k}, \tilde{\mathbf{W}}^{\text{red}}, \tilde{\tau})$ 
for  $i$  in the set of vertices do                       // vertices are in topological order
    if  $i$  is a source then
         $B_i \leftarrow \text{Id}_{d_i}$ 
    else if  $i$  is a sink then
         $C_i \leftarrow \text{Id}_{d_i}$ 
    else
         $\hat{B}_i \leftarrow \text{hstack}(W_e B_{s(e)} : t(e) = i)$            // concatenate matrices horizontally
         $B_i \leftarrow \text{full\_rank}(\hat{B}_i)$                                //  $B_i$  is always full rank
         $k_i \leftarrow \text{num\_col}(B_i)$                                //  $k_i \leq d_i$ 
         $C_i \leftarrow \text{left\_inverse}(B_i)$                          //  $C_i \in \mathbb{R}^{k_i \times d_i}$  exists since  $B_i$  is full rank
         $\tilde{\tau}_i \leftarrow C_i \circ \rho_i \circ B_i$                      // update rescaling activations
    for  $e$  such that  $t(e) = i$  do                                     // iterate through incoming edges (if any)
         $\tilde{W}_e^{\text{red}} \leftarrow C_i W_e B_{s(e)} \in \mathbb{R}^{k_i \times k_{s(e)}}$        // define reduced weights
    end
end
return  $(\mathbf{k}, \tilde{\mathbf{W}}^{\text{red}}, \tilde{\tau})$ 
    
```

APPENDIX B. PROJECTED GRADIENT DESCENT

In this appendix, we collect results related to projected gradient descent and provide a proof of Theorem 5.1. We begin by introducing a subspace of $\text{Param}(\mathcal{Q}, \mathbf{d})$ that interpolates between $\text{Param}(\mathcal{Q}, \mathbf{d})$ and $\text{Param}(\mathcal{Q}, \mathbf{d}^{\text{red}})$. Fix a neural quiver \mathcal{Q} and a dimension vector \mathbf{d} for \mathcal{Q} . The *interpolating space* $\text{Param}^{\text{int}}(\mathcal{Q}, \mathbf{d})$ is defined as the subspace of $\text{Param}(\mathcal{Q}, \mathbf{d})$ consisting of those $\mathbf{T} = (T_e)_{e \in E} \in \text{Param}(\mathcal{Q}, \mathbf{d})$ such that, for each edge, the bottom left $(d_{t(e)} - d_{t(e)}^{\text{red}}) \times d_{s(e)}^{\text{red}}$ block of T_e is zero. The following lemma is a straightforward consequence of Algorithm 1.

Lemma B.1. *Let $\mathbf{W} \in \text{Param}(\mathcal{Q}, \mathbf{d})$ and let $\mathbf{Q} \in O(\mathbf{d}^{\text{hid}})$ be the parameter symmetry in produced by Algorithm 1. Then $\mathbf{T} = \mathbf{Q}^{-1} \cdot \mathbf{W}$ belongs to the interpolating space $\text{Param}^{\text{int}}(\mathcal{Q}, \mathbf{d})$.*

Recall that $\text{Inc}_i : \mathbb{R}^{d_i^{\text{red}}} \hookrightarrow \mathbb{R}^{d_i}$ denotes the inclusion into the first d_i^{red} coordinates. The proof of the next lemma is an elementary verification.

Lemma B.2. *Let $\mathbf{T} \in \text{Param}^{\text{int}}(\mathcal{Q}, \mathbf{d})$. For each edge e , there is a matrix $\bar{T}_e \in \mathbb{R}^{d_{t(e)}^{\text{red}} \times d_{s(e)}^{\text{red}}}$ such that: $T_e \circ \text{Inc}_{s(e)} = \text{Inc}_{t(e)} \circ \bar{T}_e$. In particular, the image of $\mathbb{R}^{d_{s(e)}^{\text{red}}}$ under T_e is contained in $\mathbb{R}^{d_{t(e)}^{\text{red}}}$, that is: $T_e \left(\mathbb{R}^{d_{s(e)}^{\text{red}}} \right) \subseteq \mathbb{R}^{d_{t(e)}^{\text{red}}}$.*

Hence, each T_e is block upper triangular with \bar{T}_e appearing as the top left block: $T_e = \begin{bmatrix} \bar{T}_e & * \\ 0 & * \end{bmatrix}$.

Moreover, the tuple $(\bar{T}_e)_{e \in E}$ belongs to $\text{Param}(\mathcal{Q}, \mathbf{d}^{\text{red}})$. To explain the sense in which $\text{Param}^{\text{int}}(\mathcal{Q}, \mathbf{d})$ interpolates between $\text{Param}(\mathcal{Q}, \mathbf{d})$ and $\text{Param}(\mathcal{Q}, \mathbf{d}^{\text{red}})$, consider the following diagram

$$\text{Param}(\mathcal{Q}, \mathbf{d}^{\text{red}}) \begin{array}{c} \xrightarrow{\iota_2} \\ \xleftarrow{q_2} \end{array} \text{Param}^{\text{int}}(\mathcal{Q}, \mathbf{d}) \begin{array}{c} \xrightarrow{\iota_1} \\ \xleftarrow{q_1} \end{array} \text{Param}(\mathcal{Q}, \mathbf{d})$$

- The map ι_1 is the natural inclusion.
- The projection $q_1 : \text{Param}(\mathcal{Q}, \mathbf{d}) \rightarrow \text{Param}^{\text{int}}(\mathcal{Q}, \mathbf{d})$ takes a tuple $\mathbf{W} \in \text{Param}(\mathcal{Q}, \mathbf{d})$ and zeros to lower left $(d_i - d_i^{\text{red}}) \times d_j^{\text{red}}$ block of each W_e . Note that $\text{Proj} = \iota_1 \circ q_1$, and the transpose of q_1 is the inclusion ι_1 .
- The inclusion $\iota_2 : \text{Param}(\mathcal{Q}, \mathbf{d}^{\text{red}}) \hookrightarrow \text{Param}^{\text{int}}(\mathcal{Q}, \mathbf{d})$ takes \mathbf{X} to the tuple whose matrix corresponding to e is obtained from X_e by padding with $d_{t(e)} - d_{t(e)}^{\text{red}}$ rows of zeros and $d_{s(e)} - d_{s(e)}^{\text{red}}$ columns of zeros: $\iota_2(\mathbf{X})_e = \begin{bmatrix} X_e & 0 \\ 0 & 0 \end{bmatrix}$.
- The projection $q_2 : \text{Param}^{\text{int}}(\mathcal{Q}, \mathbf{d}) \rightarrow \text{Param}(\mathcal{Q}, \mathbf{d}^{\text{red}})$ takes a tuple \mathbf{T} in the interpolating space, and extracts the top left $d_{t(e)}^{\text{red}} \times d_{s(e)}^{\text{red}}$ block of each matrix T_e . In other words, $q_2(\mathbf{T}) = \bar{\mathbf{T}}$. The transpose of q_2 is the inclusion ι_2 .

Finally, we set $\iota = \iota_1 \circ \iota_2 : \text{Param}(\mathcal{Q}, \mathbf{d}^{\text{red}}) \hookrightarrow \text{Param}(\mathcal{Q}, \mathbf{d})$ to be the inclusion of $\text{Param}(\mathcal{Q}, \mathbf{d}^{\text{red}})$ into $\text{Param}(\mathcal{Q}, \mathbf{d})$. This is defined in essentially the same way as ι_2 . To state the next result, recall the set-up of Section 5.2. Namely, fix a dimension vector \mathbf{d} and radial activation functions $\boldsymbol{\rho} = (\rho_i : \mathbb{R}^{d_i} \rightarrow \mathbb{R}^{d_i})_{i \in I}$. For any batch of training data, we have the loss functions $\mathcal{L} : \text{Param}(\mathcal{Q}, \mathbf{d}) \rightarrow \mathbb{R}$ and $\mathcal{L}_{\text{red}} : \text{Param}(\mathcal{Q}, \mathbf{d}^{\text{red}}) \rightarrow \mathbb{R}$.

Lemma B.3. *We have the following:*

- (1) *The inclusion $\iota = \iota_1 \circ \iota_2 : \text{Param}(\mathcal{Q}, \mathbf{d}^{\text{red}}) \hookrightarrow \text{Param}(\mathcal{Q}, \mathbf{d})$ intertwines the loss functions; that is, we have: $\mathcal{L} \circ \iota = \mathcal{L}_{\text{red}}$.*
- (2) *We have that $\mathcal{L} \circ \iota_1 = \mathcal{L}_{\text{red}} \circ q_2$. In other words, the following diagram commutes:*

$$\begin{array}{ccc} \text{Param}^{\text{int}}(\mathcal{Q}, \mathbf{d}) & \xrightarrow{q_2} \twoheadrightarrow & \text{Param}(\mathcal{Q}, \mathbf{d}^{\text{red}}) \\ \downarrow \iota_1 & & \downarrow \mathcal{L}_{\text{red}} \\ \text{Param}(\mathcal{Q}, \mathbf{d}) & \xrightarrow{\mathcal{L}} & \mathbb{R} \end{array}$$

- (3) *For any $\mathbf{T} \in \text{Param}^{\text{int}}(\mathcal{Q}, \mathbf{d})$, we have: $q_1 \left(\nabla_{\iota_1(\mathbf{T})} \mathcal{L} \right) = \iota_2 \left(\nabla_{q_2(\mathbf{T})} \mathcal{L}_{\text{red}} \right)$.*

Proof. We begin with some set-up. We fix a topological order of the vertices of \mathcal{Q} . For each vertex i , we set $\pi_i : \mathbb{R}^{d_i} \rightarrow \mathbb{R}^{d_i^{\text{red}}}$ to be the projection into the first d_i^{red} coordinates. Observe that, if $\mathbf{X} \in \text{Param}(\mathcal{Q}, \mathbf{d}^{\text{red}})$, then $\iota(\mathbf{X})_e = \text{Inc}_{t(e)} \circ X_e \circ \pi_{s(e)}$ for each edge e . For the first claim, it suffices to verify that, for any \mathbf{X} in $\text{Param}(\mathcal{Q}, \mathbf{d}^{\text{red}})$, the feedforward functions of \mathbf{X} and $\iota(\mathbf{X})$ coincide. To this end, for any vertex i , we set F_i to be the i -th partial feedforward function of the \mathcal{Q} -neural network $(\mathbf{d}, \iota(\mathbf{X}), \rho)$ and G_i to be the i -th partial feedforward function of the \mathcal{Q} -neural network $(\mathbf{d}^{\text{red}}, \mathbf{X}, \rho^{\text{red}})$. We prove by induction that the following identity holds:

$$(B.1) \quad F_i = \text{Inc}_i \circ G_i$$

for any vertex i . Indeed, the identity is true for all source vertices since $d_i = d_i^{\text{red}}$ for such vertices. For the induction step, we compute:

$$\begin{aligned} F_i &= \rho_i \left(\sum_{e \in t^{-1}(i)} \iota(\mathbf{X})_e \circ F_{s(e)} \right) = \rho_i \left(\sum_{e \in t^{-1}(i)} \text{Inc}_i \circ X_e \circ \pi_{s(e)} \circ \text{Inc}_{s(e)} \circ G_{s(e)} \right) \\ &= \rho_i \circ \text{Inc}_i \left(\sum_{e \in t^{-1}(i)} X_e \circ G_{s(e)} \right) = \text{Inc}_i \circ \rho_i^{\text{red}} \left(\sum_{e \in t^{-1}(i)} X_e \circ G_{s(e)} \right) = \text{Inc}_i \circ G_i \end{aligned}$$

where the first equality follows from the definition of the neural function of $(\iota(\mathbf{X}), \mathbf{a})$, the second from the induction hypothesis and the fact that $\iota(\mathbf{X})_e = \text{Inc}_{t(e)} \circ X_e \circ \pi_{s(e)}$ for each edge e , the third from the linearity of Inc_i and the fact that $\pi_i \circ \text{Inc}_i = \text{Id}_{d_i^{\text{red}}}$ for each vertex i , the fourth from the commutativity property of radial functions with inclusions (Lemma A.5), and the last from the definition of the neural function of $(\mathbf{X}, \mathbf{a}|\mathbf{X})$. The second claim follows from an argument similar to the one used to prove the first claim, using the fact that $T_e \circ \text{Inc}_{s(e)} = \text{Inc}_{t(e)} \circ \bar{T}_e$ and $\rho_i \circ \text{Inc}_i = \text{Inc}_c \circ \rho_i^{\text{red}}$. The proof of the last claim is a straightforward computation (omitted) involving the commutative diagram appearing in the second claim. \square

We now restate Theorem 5.1 and give a proof.

Theorem 5.1. *Let $\mathbf{W} \in \text{Param}(\mathcal{Q}, \mathbf{d})$, and let $\mathbf{W}^{\text{red}}, \mathbf{Q}, \mathbf{T}$ be as above. For any $k \geq 0$, we have⁴:*

$$\gamma^k(\mathbf{W}) = \mathbf{Q} \cdot \gamma^k(\mathbf{T}) \quad \gamma_{\text{proj}}^k(\mathbf{T}) = \gamma_{\text{red}}^k(\mathbf{W}^{\text{red}}) + (\mathbf{T} - \mathbf{W}^{\text{red}}).$$

⁴More precisely, the second equality is $\gamma_{\text{proj}}^k(\mathbf{T}) = \iota(\gamma_{\text{red}}^k(\mathbf{W}^{\text{red}})) + \mathbf{T} - \iota(\mathbf{W}^{\text{red}})$ where $\iota : \text{Param}(\mathcal{Q}, \mathbf{d}^{\text{red}}) \hookrightarrow \text{Param}(\mathcal{Q}, \mathbf{d})$ is the natural inclusion. See Appendix B.

Proof. The action of \mathbf{Q} on $\text{Param}(\mathcal{Q}, \mathbf{d})$ is an orthogonal transformation, and does not change the feedforward function. Hence the first equality in the statement of the theorem follows from a basic interaction of orthogonal transformations with gradient descent (see Proposition 2.5 of [GvLW22]). For the second equality of the theorem, we proceed by induction. As noted in Footnote 3, the second equality is actually $\gamma_{\text{proj}}^k(\mathbf{T}) = \iota(\gamma_{\text{red}}^k(\mathbf{V})) + \mathbf{T} - \iota(\mathbf{V})$. The base case $k = 0$ is immediate. For the induction step, let $k > 0$ and set

$$\mathbf{Z}^{(k)} := \iota(\gamma_{\text{red}}^k(\mathbf{V})) + \mathbf{T} - \iota(\mathbf{V}).$$

Each $\mathbf{Z}^{(k)}$ belongs to $\text{Param}^{\text{int}}(\mathcal{Q}, \mathbf{d})$, so $i_1(\mathbf{Z}^{(k)}) = \mathbf{Z}^{(k)}$. Moreover, $\overline{\mathbf{Z}^{(k)}} = q_2(\mathbf{Z}^{(k)}) = \gamma_{\text{red}}^k(\mathbf{V})$. We compute:

$$\begin{aligned} \gamma_{\text{proj}}^{k+1}(\mathbf{T}) &= \gamma_{\text{proj}}(\gamma_{\text{proj}}^k(\mathbf{T})) = \gamma_{\text{proj}}(\iota(\gamma_{\text{red}}^k(\mathbf{V})) + \mathbf{T} - \iota(\mathbf{V})) \\ &= \iota(\gamma_{\text{red}}^k(\mathbf{V})) + \mathbf{T} - \iota(\mathbf{V}) - \text{Proj}\left(\nabla_{\iota(\gamma_{\text{red}}^k(\mathbf{V})) + \mathbf{T} - \iota(\mathbf{V})} \mathcal{L}\right) \\ &= \iota(\gamma_{\text{red}}^k(\mathbf{V})) - \iota_1 \circ q_1\left(\nabla_{i_1(\mathbf{Z}^{(k)})} \mathcal{L}\right) + \mathbf{T} - \iota(\mathbf{V}) \\ &= \iota(\gamma_{\text{red}}^k(\mathbf{V})) - \iota_1 \circ \iota_2\left(\nabla_{q_2(\mathbf{Z}^{(k)})} \mathcal{L}_{\text{red}}\right) + \mathbf{T} - \iota(\mathbf{V}) \\ &= \iota\left(\gamma_{\text{red}}^k(\mathbf{V}) - \nabla_{\gamma_{\text{red}}^k(\mathbf{V})} \mathcal{L}_{\text{red}}\right) + \mathbf{T} - \iota(\mathbf{V}) = \iota\left(\gamma_{\text{red}}^{k+1}(\mathbf{V})\right) + \mathbf{T} - \iota(\mathbf{V}) \end{aligned}$$

The second equality invokes the induction hypothesis, the third equality uses the definition of the projected gradient descent map γ_{proj} , the fourth equality relies on the interaction between the gradient and orthogonal transformations (see [GvLW22, Proposition 2.5]), the fifth and sixth equalities follow from Lemma B.3 above, and the last equality uses the definition of the gradient descent map γ_{red} . \square

Remark B.4. We note that the proof of Theorem 5.1 parallels that of Theorem 7 of [GvLW22]. The main differences are (1) the different structure of $\text{Param}(\mathcal{Q}, \mathbf{d}^{\text{red}})$ as a subspace of $\text{Param}(\mathcal{Q}, \mathbf{d})$, and (2) the recursive arguments related to a topological order of the vertices.

APPENDIX C. THE QR DECOMPOSITION FOR QUIVER REPRESENTATIONS

In this appendix, we summarize the mathematical formalism of quiver representations, and its relation to the results of this paper. We then prove a theoretical result on an analogue of the QR decomposition for representations of an acyclic quiver.

C.1. Basic definitions. Let $\mathcal{Q} = (I, E)$ be a quiver and \mathbf{d} a dimension vector for \mathcal{Q} , i.e., an assignment of a non-negative integer d_i to each vertex. A *representation* of \mathcal{Q} consists of a matrix for each edge, where the matrix A_e corresponding to an edge $\bullet \xrightarrow{s \quad e \quad t} \bullet$ must be of size $d_t \times d_s$. Therefore, a representation can be regarded as a tuple of matrices $\mathbf{A} = (A_e)_{e \in E}$ indexed by the set of edges, where $A_e \in \mathbb{R}^{d_{t(e)} \times d_{s(e)}}$. The set $\text{Rep}(\mathcal{Q}, \mathbf{d})$ of all possible representations of a quiver \mathcal{Q} with dimension vector \mathbf{d} is the direct sum of matrix spaces, and hence a vector space:

$$\text{Rep}(\mathcal{Q}, \mathbf{d}) = \bigoplus_{e \in E} \mathbb{R}^{d_{t(e)} \times d_{s(e)}}.$$

We see that the spaces $\text{Param}(\mathcal{Q}, \mathbf{d})$ and $\text{Rep}(\mathcal{Q}, \mathbf{d})$ are the same, so (if \mathcal{Q} is a neural quiver) the space of parameters for \mathcal{Q} -neural networks with widths \mathbf{d} is the same as the space of representations of \mathcal{Q} with dimension vector \mathbf{d} . The former notation emphasizes the relation with neural networks and their parameters, while the latter emphasizes the relation with representation theory. Let \mathbf{A} be a representation of \mathcal{Q} of dimension vector \mathbf{d} . A *subrepresentation* of \mathbf{A} is a representation $\mathbf{B} = (B_e)_{e \in E}$ with dimension vector $\mathbf{k} = (k_i)$, together with an injective map $\alpha_i : \mathbb{R}^{k_i} \hookrightarrow \mathbb{R}^{d_i}$ for each vertex such that, for each edge e , we have: $A_e \circ \alpha_{s(e)} = \alpha_{t(e)} \circ B_e$. In particular, $k_i \leq d_i$ for each vertex i .

A representation of a quiver may be viewed as a tuple of matrices indexed by vertices rather than by edges, as we now explain. First, given a dimension vector \mathbf{d} for \mathcal{Q} , recall the *incoming dimension* $d_{\rightarrow i}$ at a vertex i to be the sum of all the dimension vectors at vertices with an edge to i . In symbols, $d_{\rightarrow i} := \sum_{j \rightarrow i} d_j$, where the sum is over the subset $s(t^{-1}(i))$ of I . By convention, $d_{\rightarrow i} = 0$ if i is a source. Fix an enumeration $E = \{e_1, \dots, e_{|E|}\}$ of the edges of \mathcal{Q} . Let \mathbf{A} be a representation of \mathcal{Q} with dimension vector \mathbf{d} . For each non-source vertex i , set:

$$(C.1) \quad A_{\rightarrow i} = \begin{bmatrix} A_{e_{k_1}} & \dots & A_{e_{k_r}} \end{bmatrix} \in \mathbb{R}^{d_i \times d_{\rightarrow i}}$$

where $\{e_{k_1}, \dots, e_{k_r}\} = t^{-1}(i)$ is the set of edges with target i , with $k_1 \leq \dots \leq k_r$ (using the enumeration of the edges fixed above). Hence we obtain a map $\text{Rep}(\mathcal{Q}, \mathbf{d}) \xrightarrow{\sim} \bigoplus_{i \in I} \mathbb{R}^{d_i \times d_{\rightarrow i}}$ taking a representation \mathbf{A} to the tuple⁵ $(A_{\rightarrow i})_{i \in I}$. This map is in fact an isomorphism.

C.2. The QR decomposition. We are now ready to state the QR-decomposition result for quiver representations. Our construction is very general; however, in its simplest form, the QR decomposition for quiver representations is not aligned with the practical purpose of model compression, and hence its appearance in the appendix rather than the main text. The two procedures are nonetheless closely related, and we discuss these connections.

Let $\mathcal{Q} = (I, E)$ be a quiver, and let \mathbf{d} be a dimension vector for \mathcal{Q} . Recall from Section 5.1 the product of orthogonal groups $O(\mathbf{d}^{\text{hid}}) = \prod O(d_i)$ where the product runs over all hidden vertices (i.e., vertices that are neither sources nor sinks). This group acts on $\text{Param}(\mathcal{Q}, \mathbf{d}) = \text{Rep}(\mathcal{Q}, \mathbf{d})$ by orthogonal change-of-basis transformations.

⁵Technically, the index runs over non-source vertices in I , since A_i is not defined if i is a source.

Algorithm 4: QR decomposition for quiver representations.

```

input :  $\mathbf{A} = (A_e \in \mathbb{R}^{d_{t(e)} \times d_{s(e)}}) \in \text{Rep}(\mathcal{Q}, \mathbf{d})$ 
output:  $\mathbf{Q} \in O(\mathbf{d}^{\text{hid}})$  ,  $\mathbf{R} \in \text{Rep}(\mathcal{Q}, \mathbf{d})$ 
 $\mathbf{Q}, \mathbf{R} \leftarrow [], []$  // Initialize output matrix lists
for  $i$  in  $I$  do // Iterate through the vertices
  if  $i$  is not a source or a sink then
     $M = \text{hstack}(A_e Q_{s(e)} : t(e) = i)$  // Form the matrix  $M = A_{\rightarrow i}$ 
     $Q_i, R_{\rightarrow i} \leftarrow \text{QR-decomp}(M)$  // QR decomposition
    Append  $Q_i$  to  $\mathbf{Q}$ 
    for  $e$  such that  $t(e) = i$  do // Iterate through the incoming edges
       $R_e = \text{extract}(R_{\rightarrow i}, e)$  // Extract  $R_e$  from the matrix  $R_{\rightarrow i}$ 
      Append  $R_e$  to  $\mathbf{R}$ 
    end
  else if  $i$  is a sink then
    for  $e$  such that  $t(e) = i$  do // Iterate through the incoming edges
      Append  $R_e \leftarrow A_e Q_{s(e)}$  to  $\mathbf{R}$  // Define  $R_e$ 
    end
  end
end
return:  $\mathbf{Q}, \mathbf{R}$ 

```

Proposition C.1. *Let \mathcal{Q} be an acyclic quiver with no double edges. Let \mathbf{A} be a representation of \mathcal{Q} with dimension vector \mathbf{d} . Then there exist $\mathbf{Q} = (Q_i)_{i \in I} \in O(\mathbf{d}^{\text{hid}})$ and $\mathbf{R} = (R_e)_{e \in E} \in \text{Rep}(\mathcal{Q}, \mathbf{d})$ such that*

$$\mathbf{A} = \mathbf{Q} \cdot \mathbf{R},$$

and, moreover, for each non-source and non-sink vertex i , the matrix $R_{\rightarrow i}$ is upper-triangular.

Proof. The proof is constructive, based on Algorithm 4. The algorithm takes as input a representation \mathbf{A} of dimension vector \mathbf{d} and outputs $\mathbf{Q}, \mathbf{R} = \text{QRDecomp}(\mathbf{A})$, where $\mathbf{Q} \in O(\mathbf{d}^{\text{hid}})$ is an element of the change-of-basis symmetry group and $\mathbf{R} \in \text{Rep}(\mathcal{Q}, \mathbf{d})$ is a representation of \mathcal{Q} with dimension vector \mathbf{d} . To see that \mathbf{Q} and \mathbf{R} have the desired properties, first note that $R_{\rightarrow i}$ is indeed upper-triangular for every non-sink vertex i , and Q_i is indeed orthogonal for every i . Next, the defining property of the topological ordering implies that, by the time the algorithm reaches a vertex i , the matrix $A_{\rightarrow i}$ has been updated to $A'_{\rightarrow i} = A_{\rightarrow i} \circ \text{Diag}(Q_{s(e_{k_1})}, Q_{s(e_{k_2})}, \dots, Q_{s(e_{k_r})})$, where $t^{-1}(i) = \{e_{k_1}, \dots, e_{k_r}\}$, with $k_1 \leq \dots \leq k_r$. If i is not a sink, the algorithm computes the QR decomposition of this matrix $A'_{\rightarrow i}$ to obtain Q_i and $R_{\rightarrow i}$. Hence:

$$\begin{aligned} (\mathbf{Q} \cdot \mathbf{R})_{\rightarrow i} &= Q_i \circ R_{\rightarrow i} \circ \text{Diag}(Q_{s(e_{k_1})}^{-1}, \dots, Q_{s(e_{k_r})}^{-1}) = A'_{\rightarrow i} \circ \text{Diag}(Q_{s(e_{k_1})}^{-1}, \dots, Q_{s(e_{k_r})}^{-1}) \\ &= A_{\rightarrow i} \circ \text{Diag}(Q_{s(e_{k_1})}, \dots, Q_{s(e_{k_r})}) \circ \text{Diag}(Q_{s(e_{k_1})}^{-1}, \dots, Q_{s(e_{k_r})}^{-1}) = A_{\rightarrow i} \end{aligned}$$

On the other hand, if i is a sink, then $R_{\rightarrow i} = A'_{\rightarrow i}$ and $Q_i = \text{Id}_{d_i}$. As similar calculation as above shows that $(\mathbf{Q} \cdot \mathbf{R})_{\rightarrow i} = A_{\rightarrow i}$. We note that the representation \mathbf{A} is determined by the matrices $A_{\rightarrow i}$ as i ranges over the non-source vertices. This finishes the proof. \square

C.3. Relation to neural networks. We now explain the relation between Algorithm 1 and Algorithm 4. First, we note that a more general version of Proposition C.1 holds, namely, each representation admits a decomposition $\mathbf{W} = \mathbf{Q} \cdot \mathbf{R}$, where each Q_i is orthogonal, and each $R_{\rightarrow i}$ becomes upper triangular after an appropriate permutation of the columns. Indeed, the only necessary modifications to Algorithm 4 are that one must:

- (1) fix a permutation matrix $P_i \in \mathbb{R}^{d_{\rightarrow i} \times d_{\rightarrow i}}$ for each non-source vertex i ,
- (2) perform $W_i \leftarrow W_i \circ P_i^{-1}$ before computing the QR decomposition $W_i = Q_i \circ R'_i$, and
- (3) set $R_{\rightarrow i} = R'_{\rightarrow i} \circ P_i$.

We now consider, for each non-sink vertex i , the permutation of the standard basis of $\mathbb{R}^{d_{\rightarrow i}} = \mathbb{R}^{d_{j_1}} \oplus \dots \oplus \mathbb{R}^{d_{j_r}}$ in which all the standard basis vectors of $\mathbb{R}^{d_{\rightarrow i}^{\text{red}}} = \mathbb{R}^{d_{j_1}^{\text{red}}} \oplus \dots \oplus \mathbb{R}^{d_{j_r}^{\text{red}}}$ appear first, in order, before the remaining basis vectors⁶. Hence we have a permutation matrix $P_i \in \mathbb{R}^{d_{\rightarrow i} \times d_{\rightarrow i}}$ for each non-sink vertex i . We now apply the modification of Algorithm 4 described above to produce \mathbf{Q} and \mathbf{R} . The matrices \mathbf{Q} will be the same as those in Algorithm 1. For each edge e , take W_e^{red} to be the top left $d_{t(e)} \times d_{s(e)}$ block of each R_e . These are the matrices $\mathbf{W}_e^{\text{red}}$ appearing in Algorithm 1.

Let \mathcal{Q} be a neural quiver and let \mathbf{d} be a dimension vector for \mathcal{Q} . Recall from Section 5 that for any activation functions ρ and any batch of training data we have a loss function $\mathcal{L} : \text{Param}(\mathcal{Q}, \mathbf{d}) \rightarrow \mathbb{R}$ and gradient descent map $\gamma : \text{Param}(\mathcal{Q}, \mathbf{d}) \rightarrow \text{Param}(\mathcal{Q}, \mathbf{d})$. (These maps can be equivalently regarded on $\text{Rep}(\mathcal{Q}, \mathbf{d})$.) The following result shows that gradient descent optimization starting at \mathbf{W} is equivalent to gradient descent optimization starting at \mathbf{R} .

Corollary C.2. *Let \mathbf{W} be a representation of \mathcal{Q} and let $\mathbf{W} = \mathbf{Q} \cdot \mathbf{R}$ be its QR decomposition. Fix radial rescaling activations ρ . Then, for any $k \geq 0$, we have:*

$$\gamma^k(\mathbf{W}) = \mathbf{Q} \cdot \gamma^k(\mathbf{R})$$

Sketch of proof. Note that the action of \mathbf{Q} on $\text{Rep}(\mathcal{Q}, \mathbf{d})$ is an orthogonal transformation. Moreover, this action does not change the feedforward function, due to the fact that orthogonal transformations commute with radial functions (see Lemma A.5). Consequently, the action of \mathbf{Q} commutes with any number of steps of gradient descent (see Lemma 21 of [GvLW22]). \square

⁶To be more explicit, let $\epsilon_1^{(1)}, \dots, \epsilon_{d_{j_1}^{\text{red}}}^{(1)}$ be the standard basis of $\mathbb{R}^{d_{j_1}^{\text{red}}}$, let $\epsilon_1^{(2)}, \dots, \epsilon_{d_{j_2}^{\text{red}}}^{(2)}$ be the standard basis of $\mathbb{R}^{d_{j_2}^{\text{red}}}$, and so forth. These combine, in order, to produce the standard basis of $\mathbb{R}^{d_{\rightarrow i}^{\text{red}}} = \mathbb{R}^{d_{j_1}^{\text{red}}} \oplus \dots \oplus \mathbb{R}^{d_{j_r}^{\text{red}}}$. Consider the new basis of $\mathbb{R}^{d_{\rightarrow i}}$ starting with $\epsilon_1^{(1)}, \dots, \epsilon_{d_{j_1}^{\text{red}}}^{(1)}, \epsilon_1^{(2)}, \dots, \epsilon_{d_{j_2}^{\text{red}}}^{(2)}, \dots, \epsilon_1^{(r)}, \dots, \epsilon_{d_{j_r}^{\text{red}}}^{(r)}$ and ending with the remaining standard basis vectors (in any order).